Abundant Phenotypic Parallelism, Incomplete Lineage Sorting, and Introgression in Open-Habitat Chats

Niloofar Alaei Kakhki [1], Manuel Schweizer [2,3], Dave Lutgen [3,1,4], Rauri C. K. Bowie [5,6], Hadoram Shirihai [2], Alexander Suh [7,8], Holger Schielzeth [1,9], Reto Burri [4,3,1]

[1] Department of Population Ecology, Institute of Ecology and Evolution, Friedrich-Schiller-University Jena, Jena, Germany

[2] Natural History Museum Bern, Bern, Switzerland

[3] Institute of Ecology and Evolution, University of Bern, Bern, Switzerland

[4] Swiss Ornithological Institute, Sempach, Switzerland

[5] Museum of Vertebrate Zoology, University of California, Berkeley, USA

[6] Department of Integrative Biology, University of California, Berkeley, USA

[7] School of Biological Sciences, University of East Anglia, Norwich, United Kingdom

[8] Department of Organismal Biology – Systematic Biology (EBC), Science for Life Laboratory, Evolutionary Biology Centre, Uppsala University, Uppsala, Sweden

[9] German Centre for Integrative Biodiversity Research (iDiv), Halle-Jena-Leipzig, Leipzig, Germany

Correspondence

Niloofar Alaei Kakhki, Department of Population Ecology, Institute of Ecology and Evolution, Friedrich-Schiller-University Jena, Dornburger Str. 159, D-07743 Jena, Germany
Email: niloofar.alaei.kakhki@uni-jena.de

Reto Burri, Swiss Ornithological Institute, Seerose 1, CH-6204 Sempach.
Email: reto.burri@vogelwarte.ch

Abstract

Insights into the processes underpinning the evolution of phenotypic parallelism contribute to our understanding of the contributions of ancestral, introgressed, and novel genetic variation to phenotypic evolution. Phylogenomic analyses characterizing genome-wide gene tree heterogeneity can provide first clues about the extent of ILS and of introgression and thereby into the potential of these processes or (in their absence) the need to invoke novel mutations to underpin phenotypic parallelism. Here, we were interested in understanding the trajectories along which phenotypic parallelism may have evolved in open-habitat chats (wheatears of the genus *Oenanthe* and their relatives). To this end, based on whole-genome resequencing data from 50 taxa of 44 species, we established the species tree, characterized gene tree heterogeneity, and investigated the footprints of ILS and introgression within the latter. The species tree corroborates the evidence for abundant phenotypic parallelism, especially in wheatears. The high levels of gene tree heterogeneity in wheatears are explained by ILS alone only for 30% of internal branches. For multiple branches with high gene tree heterogeneity, D-statistics and phylogenetic networks identified footprints of introgression. Finally, long branches without extensive ILS between clades sporting similar phenotypes provide suggestive evidence for a role of novel mutations in the evolution of these phenotypes. Together, our results suggest that phenotypic parallelism in open-habitat chats evolved along diverse trajectories and highlight that phenotypic diversification is often complex and best depicted as a network of interacting lineages.

Introduction

Molecular phylogenetics has unveiled many previously unknown examples of phenotypic parallelism – here defined as a pattern in which non-sister species spread across the phylogeny are phenotypically more similar to each other than to their respective sister species. Under such an evolutionary outcome, species relationships based on morphometrics, coloration, behavior, or other ecological traits are discordant with the history of descent reflected in the species tree (Aliabadian et al. 2012; Elmer and Meyer 2011; Jarvis et al. 2014; Martin and Orgogozo 2013; Paterson et al. 2020; Schweizer et al. 2019a; Schweizer et al. 2019b; Stern 2013). While the many observations of such discordances across diverse species assemblages witness of the abundance of phenotypic parallelism, insights into the underlying processes remain more elusive.

Phylogenetic information from genome sequencing data now provides unprecedented power to consolidate patterns of phenotypic parallelism and obtain insights into the processes underlying them. Many published examples of putative phenotypic parallelism are yet derived from interpretations of traits mapped across phylogenies using a single or a restricted number of genetic markers (Aliabadian et al. 2012; Brusatte et al. 2015; Colosimo et al. 2005; Cresko et al. 2004; Stern 2013). Since phylogenetic relationships at different positions in the genome, referred to as 'gene trees', can vary substantially, many gene trees inevitably deviate from the species' history of descent reflected in the species tree (Degnan and Rosenberg 2006; Toews and Brelsford 2012). Hence, the mismatch of single gene trees with phenotypic similarities alone does not provide conclusive evidence for phenotypic parallelism (Degnan and Rosenberg 2006; Doyle 1997; Lamers et al. 2012). Confirming instances of phenotypic parallelism, therefore, requires species tree reconstructions from genome-wide variation. Once the evidence for phenotypic parallelism is corroborated by the species tree, we can move on to investigate processes underlying gene tree heterogeneity that, in part, can underpin phenotypic parallelism.

Phenotypic parallelism can evolve in three ways: First, under phenotypic parallelism *sensu stricto*, phenotypic similarities evolve through independent mutations in the same or different genes (Arendt and Reznick 2008; Christin et al. 2010; Gompel and Prud'homme 2009; Martin and Orgogozo 2013; Stern 2013). In Mexican cavefish (*Astyanax mexicanus*), for instance, the phenotypic parallelism of decolored brown phenotypes and albinism in separate caves occurred through different mutations in the MC1R and OCA2 genes, respectively (Gross et al. 2009; Protas et al. 2006; Stahl and Gross 2015). Similarly, isoforms of PEPC found in C4 photosynthesis (Besnard et al. 2009; Christin et al. 2007), and similar floral traits important for pollination (Hoballah et al. 2007; Preston and Hileman 2009; Whittall et al. 2006) have evolved multiple times independently in plants.

The second, and likely most frequent process leading to phenotypic parallelism that also accounts for most gene tree heterogeneity is incomplete lineage sorting (ILS), that is, the retention

of alleles and traits that were already present in the ancestral lineage (Colosimo et al. 2005; Cresko et al. 2004; Stern 2013; Van Belleghem et al. 2018). ILS is especially prevalent in radiations characterized by large effective population sizes and fast succession of speciation events, such as, for instance, in the evolution of neoavian birds (Jarvis et al. 2014; Suh 2016; Suh et al. 2015). In such cases, a high proportion of ancestral variation may be retained over subsequent species splits and segregate in the independently evolving gene pools of daughter species (Maddison 1997). Selection or drift in non-sister species may fix the same genotype (and phenotype), while sister species may fix a different genotype/phenotype. For instance in Humans, at least 1% of the genome is genetically more similar to orangutans than to chimps due to ILS, even though these primates are characterized by small effective population sizes (Hobolth et al. 2011).

Third, in hybridizing lineages, phenotypic parallelism and gene tree heterogeneity may be underpinned by introgression that mingles genotypes and phenotypes among species (Heliconius Genome Consortium 2012; Malinsky et al. 2018; Song et al. 2011; Stryjewski and Sorenson 2017). In particular, introgression between non-sister species may result in these species being phenotypically more similar than they are to their respective sister species, such as exemplified by wing-pattern mimicry in *Heliconius* butterflies (Edelman et al. 2019; Pardo-Diaz et al. 2012) and plumage coloration of *Munia* finches (Stryjewski and Sorenson 2017) and of members of the Black-eared Wheatear (*Oenanthe hispanica*) complex (Schweizer et al. 2019a). Importantly, in an increasing number of instances, such as in *Heliconius* butterflies, Yellowstone wolves, Darwin's finches and cichlid fish in Lake Malawi and Lake Victoria, introgression has exchanged alleles between species and resulted in the formation of beneficial phenotypes (Enciso-Romero et al. 2017; Genner and Turner 2012; Grant et al. 2005; Lamers et al. 2012; Wallbank et al. 2016). Given that over the last decade genomic studies have contributed increasing evidence for the abundance of such adaptive introgression, hybridization may underpin phenotypic parallelism more often than previously appreciated (Campagna et al. 2017; Han et al. 2017; Marques et al. 2019a; Meier et al. 2018).

Multiple factors influence which of these routes specific cases of phenotypic parallelism have most likely taken. These factors include the evolutionary time scale under consideration, the speed at which successive speciation events occurred, effective population sizes, and the opportunity for genetic exchange according to biogeographic history. Waiting times for beneficial mutations are long (Barrett and Schluter 2008; Hedrick 2013; Hermisson and Pennings 2005), such that independent mutations with the same phenotypic effect are expected to be exceedingly rare (Eyre-Walker and Keightley 2007) and only over the course of millions of years may occur in sufficient number to be a source of phenotypic parallelism (Hedrick 2013). Therefore, at short evolutionary timescales, phenotypic parallelism may more often involve the recruitment of standing genetic variation (Barrett and Schluter 2008), notably from the pool of ancestral

variation segregating in extant species, or variation introgressed from other species (Stern 2013). Among young evolutionary lineages, ancestral variation is still segregating, especially if speciation events occurred rapidly. Phenotypic parallelism in such cases may occur via ILS (Jones et al. 2012; Wu et al. 2018). Furthermore, among young species, reproductive isolation may still be incomplete. Provided species overlap in time and space, the exchange of genetic variation through introgression may lead to phenotypic parallelism, too.

Although convincing examples of phenotypic parallelism include all three evolutionary trajectories, the incidence at which phenotypic parallelism occurs along each of these remains largely unknown; not least, because identifying the process involved in a particular case of phenotypic parallelism is difficult. Doing so requires mapping the genomic region underlying the phenotype in question and tracing the evolution of this genomic region across the phylogeny of the species involved. In the wild, this is often not possible.

However, phylogenomics can provide important indirect insights into the potential contribution of the abovementioned alternative processes that can underlie the development of phenotypic parallelism: First, the species tree provides first clues on whether speciation events occurred over short enough time scales for ancestral variation to be passed to descent lineages and thus remain incompletely sorted in important proportions beyond speciation events. Second, insights into the extent of ILS and presence of introgression can be gained from levels of gene tree heterogeneity (Degnan and Rosenberg 2006; Funk and Omland 2003; Jarvis et al. 2014; Nater et al. 2015; Suh 2016; Suh et al. 2015) and symmetries of gene tree frequencies (Hibbins and Hahn 2022). Gene tree heterogeneity is high under both ILS and introgression, but the two processes leave different proportions of alternative gene trees, based on which they can be distinguished (Hibbins and Hahn 2022; Sayyari and Mirarab 2018; Sayyari et al. 2018). In the presence of extensive ILS or of introgression, a parsimonious approach attributes the source of phenotypic parallelism to these processes, even though independent mutations cannot be excluded as the source of phenotypic parallelism (Colosimo et al. 2005; Cresko et al. 2004; Pardo-Diaz et al. 2012; Stryjewski and Sorenson 2017). The absence of detecting these processes, conversely, would indirectly suggest novel mutations as a potential source of phenotypic parallelism. Therefore, surveys of gene tree heterogeneity and symmetries of gene tree proportions represent a promising avenue to probe the potential of the alternative processes to contribute to phenotypic parallelism.

Here, we reconstructed the species tree and assessed the contribution of ILS and introgression to gene tree heterogeneity in open-habitat chats (genera *Campicoloides*, *Emarginata, Myrmecocichla, Oenanthe*, *Pinarochroa* and *Thamnolaea*), a monophyletic group of songbirds displaying a high incidence of phenotypic parallelism (Aliabadian et al. 2012; Mayr and Stresemann 1950; Schweizer et al. 2019a; Schweizer et al. 2019b). The phylogenetic relationships

among open-habitat chats as inferred from mitochondrial data were entirely unexpected from a morphological perspective (Aliabadian et al. 2012). Species similar in plumage coloration and other traits were often spread far apart across the mitochondrial phylogeny, suggesting that their phenotypic similarity may have evolved in parallel (Aliabadian et al. 2012; Outlaw et al. 2010; Schweizer and Shirihai 2013; Schweizer et al. 2019a; Schweizer et al. 2019b). For a limited subset of species studied, genome-wide variation (ddRAD data) confirmed the mitochondrial relationships and thus the high incidence of phenotypic parallelism (Schweizer et al. 2019b). Furthermore, hybridization resulted in substantial introgression in the *Oenanthe hispanica* complex (Schweizer et al. 2019a) and is suspected to have played a role in phenotypic and species evolution of other groups of wheatears, such as the *O. picata* complex (Panov 2005). In these instances, introgression between non-sister taxa may well explain phenotypic parallelism. However, genomic data is essential to refine the species tree and assess the incidence ILS and/or introgression across open-habitat chats.

Based on whole-genome resequencing data from 50 taxa of 47 open-habitat species (**Tab. 1**), we aimed to obtain insights into the potential roles of alternative processes in driving phenotypic parallelism in these songbirds. To this end, we (i) reconstructed the species tree, (ii) estimated gene tree variation across the genome, and (iii) explored ILS and introgression as drivers of the underlying high gene tree heterogeneity. Our results reveal a comprehensive picture of open-habitat chat evolution involving multiple instances of introgression. Footprints of ILS and introgression as well as considerable divergence times between the main clades of wheatears with phenotypic parallelism suggest that a combination of ILS, introgression and novel mutations, depending on the time scales involved most likely explains the phenotypic parallelism observed in wheatears.

Results

Sampling, Nuclear Data Preparation, and Mitogenome Assembly

To achieve an almost complete taxon sampling, we resequenced the genomes of 50 open-habitat chat taxa from 44 out of 47 currently recognized species (**Fig. 1**; **Tab. 1**). Data from *Saxicola maurus* was included as an outgroup for open-habitat chats (Sangster et al. 2010; Zuccon and Ericson 2010). We mapped the sequencing reads to the reference genome assembly of *Oenanthe melanoleuca* (Peona et al. in prep.) and followed GATK best practices for nuclear data preparation. Mapping efficiency was not correlated to the degree of evolutionary divergence from the reference genome, but data obtained from DNA extracted off museum skins mapped at a lower percentage (linear model, d_{XY}: t=-0.41, p=0.68; $tissue_{museum}$: t=-6.56, p<0.001; R^2=0.53). After mapping, sequencing coverage ranged from 4.6 x to 40.6 x, with an average coverage of 12.2 x ± 6.2 x (**Tab.**

190 **1**). We extracted mitochondrial sequence data for all 13 protein-coding genes and two rRNA
191 genes using MitoFinder 1.2 from the sequencing data.

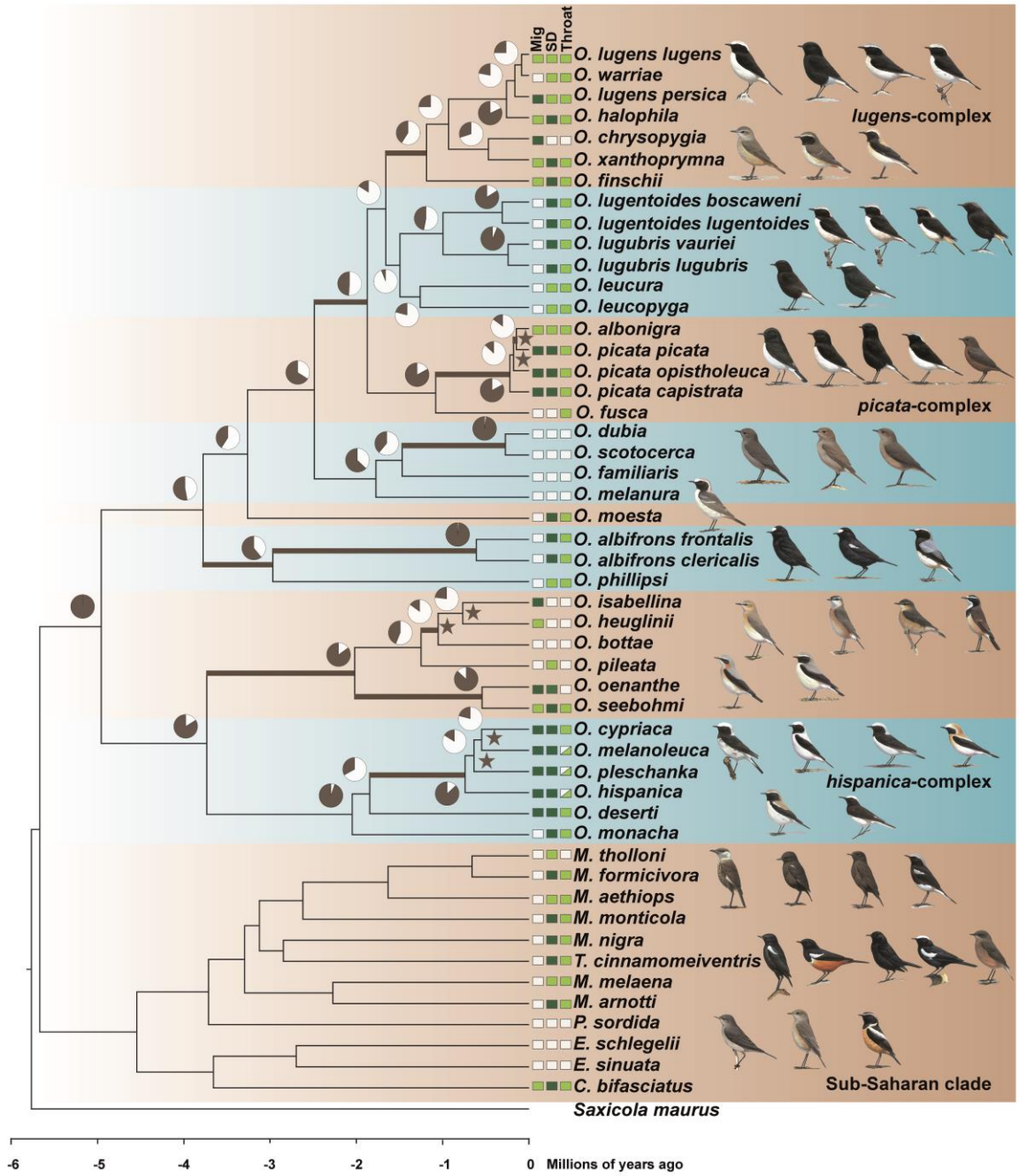

Figure 1 | Time-calibrated phylogenetic tree of open-habitat chats and levels of ILS. All nodes are supported by bootstrap values of 100. Pie charts depict the gene tree heterogeneity for each internal branch, with the brown proportion indicating the proportion of concordant gene trees (gCF). Coloured branches indicate internal branches for which ILS alone is statistically sufficient to explain the observed gene tree heterogeneity. Stars indicate branches that are in the phylogenetic anomaly zone. The character states of three selected characters: Sexual dimorphism (SD), monomorphic female-type (white), monomorphic male-type (pale green), dimorphic (dark green); Migratory behaviour (Mig), sedentary (white), short-distance migrant (pale green), long-distance migrant (dark green); and throat coloration (throat), white (white), black (pale green), and polymorphic (white and pale green). Drawing courtesy of Chris Rose (www.chrisrose-artist.co.uk) with permission from Bloomsbury Publishing Plc.

192 **Table 1 | Sampling and sequence data information**.
193

Taxon	Collection, no.[a]	Tissue	Library Type	Mapping %	Coverage
Campicoloides bifasciatus	MVZ, RSA073,	Muscle	Illumina DNA Prep Kit	99.1	8.5
Emarginata schlegelii	FMNH, 453197,	Muscle	Illumina DNA Prep Kit	99.1	9.5
Emarginata sinuata	UWMB, 95470	Muscle	ThruPLEX DNA-Seq Kit	96.7	9.7
Myrmecocichla aethiops	MVZ, 129113	Toepad	ACCEL-NGS 1S DNA Library Prep Kit	93.3	6.8
Myrmecocichla arnotti	FMNH, 468111	Toepad	Illumina DNA Prep Kit	99.3	12.8
Myrmecocichla formicivora	MVZ, RSA205	Muscle	Illumina DNA Prep Kit	98.6	8.3
Myrmecocichla melaena	A1153	Blood	ThruPLEX DNA-Seq Kit	98.8	13.3
Myrmecocichla monticola	NMBE, 1043860	Toepad	ACCEL-NGS 1S DNA Library Prep Kit	94.3	7.6
Myrmecocichla nigra	NRM, 570041	Toepad	ThruPLEX DNA-Seq Kit	94.5	7.0
Myrmecocichla tholloni	YPM, ORN95640	Toepad	ThruPLEX DNA-Seq Kit	92.1	7.3
Oenanthe (C.) dubia	FMNH, 83201	Toepad	ACCEL-NGS 1S DNA Library Prep Kit	93.0	6.8
Oenanthe (C.) familiaris	MVZ, GO866	Blood	Illumina DNA Prep Kit	99.4	13.3
Oenanthe (C.) fusca	YPM, ORN011707	Toepad	ThruPLEX DNA-Seq Kit	86.4	4.7
Oenanthe (C.) melanura	A1203	Blood	ThruPLEX DNA-Seq Kit	98.8	15.4
Oenanthe (C.) scotocerca	LACM, 61131	Toepad	ACCEL-NGS 1S DNA Library Prep Kit	96.6	8.3
Oenanthe (M.) albifrons clericalis	NRM, 558941	Toepad	ThruPLEX DNA-Seq Kit	95.4	6.3
Oenanthe (M.) albifrons frontalis	KU, 115365	Muscle	ThruPLEX DNA-Seq Kit	98.5	12.7
Oenanthe albonigra	IR-KIL-010	Blood	ThruPLEX DNA-Seq Kit	99.2	12.9
Oenanthe bottae frenata	NRM, 558917	Toepad	ThruPLEX DNA-Seq Kit	97.0	6.0
Oenanthe chrysopygia	IR-FIR-002	Blood	ThruPLEX DNA-Seq Kit	98.9	11.5
Oenanthe cypriaca	19e	Blood	Chromium Genome Library kit	99.8	40.6
Oenanthe deserti	MO-BOULMANE-2013	Blood	ThruPLEX DNA-Seq Kit	99.3	12.6
Oenanthe finschii	IR-ESF-004	Blood	ThruPLEX DNA-Seq Kit	98.9	8.7
Oenanthe halophila	3Y42902	Blood	Illumina DNA PCR-free	99.6	17.4
Oenanthe heuglinii	ZFMK, H.II.16p2.α	Dry skin	ACCEL-NGS 1S DNA Library Prep Kit	93.6	5.7

Oenanthe hispanica	E-GUI-013	Blood	Chromium Genome Library kit	99.8	15.5
Oenanthe isabellina	GR-LES-001	Blood	ThruPLEX DNA-Seq Kit	99.2	9.9
Oenanthe leucopyga leucopyga	A1137	Blood	ThruPLEX DNA-Seq Kit	98.8	10.7
Oenanthe leucura leucura	E-MAT-2012	Blood	ThruPLEX DNA-Seq Kit	99.0	9.5
Oenanthe lugens lugens	9b	Blood	ThruPLEX DNA-Seq Kit	98.7	22.0
Oenanthe lugens persica	ZMUC, 137759	Muscle	ThruPLEX DNA-Seq Kit	98.6	10.4
Oenanthe lugentoides lugentoides	NHMUK, 1965.M.12140	Toepad	ThruPLEX DNA-Seq Kit	96.9	4.6
Oenanthe lugentoides boscaweni	NHMUK, 1977.M.21.36	Toepad	ThruPLEX DNA-Seq Kit	97.2	6.8
Oenanthe lugubris lugubris	A1129	Blood	ThruPLEX DNA-Seq Kit	99.0	12.5
Oenanthe lugubris vauriei	AMNH, 461151	Toepad	ThruPLEX DNA-Seq Kit	95.9	5.3
Oenanthe melanoleuca	IT-GRA-006	Blood	Chromium Genome Library kit	99.7	12.6
Oenanthe moesta	A1109	Blood	ThruPLEX DNA-Seq Kit	98.8	12.0
Oenanthe monacha	A1174	Blood	ThruPLEX DNA-Seq Kit	99.3	17.2
Oenanthe oenanthe	GEO-VAR-002	Blood	ThruPLEX DNA-Seq Kit	99.1	12.2
Oenanthe phillipsi	YPM, ORN035210	Toepad	ThruPLEX DNA-Seq Kit	95.6	7.9
Oenanthe picata capistrata	ZMUC, 29495	Toepad	ThruPLEX DNA-Seq Kit	96.7	5.3
Oenanthe picata opistholeuca	ZMUC, 29578	Toepad	ThruPLEX DNA-Seq Kit	97.1	5.2
Oenanthe picata picata	IR-TAN-005	Blood	ThruPLEX DNA-Seq Kit	98.8	14.2
Oenanthe pileata	TCWC, 15606	Muscle	Illumina DNA Prep Kit	98.9	13.4
Oenanthe pleschanka	CN-XS-006	Blood	Chromium Genome Library kit	99.8	15.1
Oenanthe seebohmi	KA69373	Blood	ThruPLEX DNA-Seq Kit	99.2	11.2
Oenanthe warriae	12c	Blood	ThruPLEX DNA-Seq Kit	98.7	13.4
Oenanthe xanthoprymna	NHMO, 15188	Blood	ThruPLEX DNA-Seq Kit	99.0	12.9
Pinarochroa sordida	YPM, ORN80066	Toepad	ThruPLEX DNA-Seq Kit	95.4	6.5
Thamnolaea cinnamomeiventris	NRM, 20086147	Muscle	ThruPLEX DNA-Seq Kit	98.6	15.9

[a] AMNH; American Museum of Natural History; NHMUK: Natural History Museum, Tring; FMNH: Field Museum of Natural History; LACM: Natural History Museum of Los Angeles County; MVZ: Museum of Vertebrate Zoology, UC Berkeley; NHMO: Natural History Museum, University of Oslo; NRM: Naturhistoriska riksmuseet, Stockholm; TCWC: Texas A&M University Biodiversity Research and Teaching Collections; UWBM: University of Washington Burke Museum; YPM: Yale Peabody Museum; ZMUC: Zoological Museum, Natural History Museum of Denmark; ZFMK: Zoologisches Forschungsmuseum König. Samples for which no institution is indicated are part of the research group's collection.

199 To ensure that results did not depend on filtering strategy, all analyses were run with four sets of
200 differently filtered data (see Material and Methods).

201 **Species Tree Reconstruction Based on Nuclear Genomic Data**

202 We first set out to reconstruct and root the species tree based on regions of the genome least likely
203 affected by mapping biases. To this end, we extracted data from genomic intervals hosting avian
204 Benchmarking Universal Single-Copy Orthologs (BUSCOs). This resulted in data from 7,335
205 BUSCOs, with alignment lengths varying from 89,898 kb to 140,640 kb (depending on filtering
206 strategy) for ML analyses of concatenated data, respectively 2,091 BUSCOs with alignment lengths
207 varying from 10,575 kb to 15,290 kb for LD-pruned data free of interlocus recombination for
208 multispecies coalescent (MSC)-based species tree reconstruction. Results were consistent
209 between filtering strategies. Hence, we only report results based on the most stringent filtering of
210 read depth (ii, DP=5, PW=50%, MD=15%). Both, maximum likelihood (ML) analyses in IQtree2
211 based on concatenated data and MSC analyses in ASTRAL-III (based on BUSCO ML gene trees)
212 established sub-Saharan species of the genera *Campicoloides*, *Emarginata*, *Myrmecocichla*,
213 *Pinarochroa*, and *Thamnolaea* as the sister clade to all other open-habitat chats (**Fig. S1a**). For the
214 subsequent analyses we excluded the *Saxicola* outgroup and rooted the trees on the sub-Saharan
215 clade.

216 We then moved to reconstruct the species tree based on an as broad representation to the
217 genome as possible. To this end, we extracted alignments including variant and invariant sites for
218 non-overlapping 10 kb windows. We henceforth refer to these windowed data as "loci". Analyses
219 included only loci that fulfilled filtering criteria for read depth, alignment length, data missingness
220 (see Material and Methods), and absence of evidence for intra-locus recombination. Furthermore,
221 we sub-sampled filtered loci to be at least 10 kb apart to ensure free inter-locus recombination.
222 Depending on filtering strategy, this left us with 5,267-6,791 loci with total alignment lengths of
223 34,556-52,243 kb (**Tab. S1**). We identified branches in the "anomaly zone" (Degnan and
224 Rosenberg 2006) in several clades of wheatears: in the *hispanica* and *picata* complexes, and in the
225 *isabellina* clade **(Fig. 1)**. Nevertheless, the polytomy test based on local quartet supports in
226 ASTRAL-III showed no evidence for polytomies in the species tree (P = 0 for all branches). The ML
227 tree based on concatenated data and the MSC-based species tree were fully supported and in
228 agreement both with each other (except the position of T. *cinnamomeiventris* within the sub-
229 Saharan clade) and with the tree based on BUSCOs (**Fig. S1b**). Finally, a SNP-based species tree
230 estimated in SVDquartets mostly confirmed the sequence-based results (**Fig. S2**). The only three
231 disagreements (position of *O. leucura* and *O. leucopygia,* position of *O. bottae* and *O. pileata*, and
232 position of *T. cinnamomeiventris*) were poorly supported in the SNP-based analysis and are likely
233 a result of high levels of ILS under which sequence-based approaches are more accurate than
234 approaches based on SNP data alone (Chou et al. 2015).

Mitogenomic Relationships and Mito-Nuclear Discordances

We were interested in whether previously inferred relationships based predominantly on single mitochondrial genes (Alaei Kakhki et al. 2016; Aliabadian et al. 2012; Schweizer and Shirihai 2013) were supported by full mitogenomes and in inferring mito-nuclear discordances.

Mitogenomic relationships were in remarkable agreement with previously inferred phylogenetic relationships based predominantly on individual mitochondrial genes (Alaei Kakhki et al. 2016; Aliabadian et al. 2012; Schweizer and Shirihai 2013), yet showed several discordances with the species tree recovered from nuclear data (**Fig. 2**). Mito-nuclear discordances in wheatears were found in several places across the species tree but were mostly restricted to the placements of tip taxa: (i) In the *lugens* complex, nuclear data placed *O. l. persica* within the

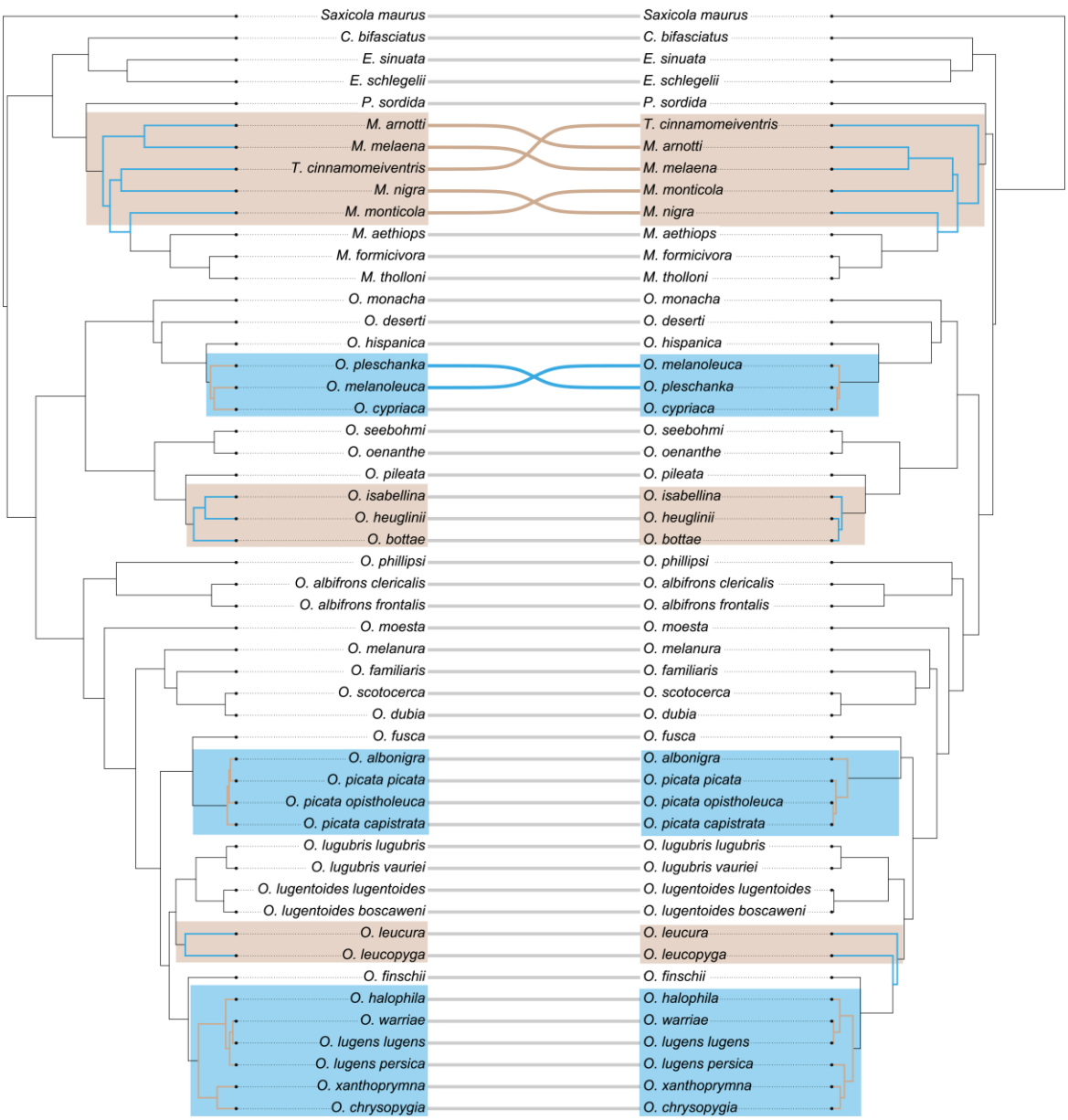

Figure 2 | Mito-nuclear discordances. Shown are the time-calibrated phylogenetic trees based on nuclear data (left) and full mitogenomes (right).

complex, whereas the mitogenome placed it with *O. xanthoprymna* and *O. chrysopygia.* (ii) In the *picata* complex, *O. albonigra* that by mitochondrial data was considered a sister taxon to the *picata* complex, was placed within the latter as a sister taxon to the phenotypically almost identical *O. p. picata* by nuclear data. (iii) In the *hispanica* complex, *O. cypriaca* was placed as sister to either *O. melanoleuca* or *O. pleschanka* in nuclear and mitogenomic data respectively. (iv) In the *isabellina* clade, *O. heuglini* as sister to either *O. isabelline* or *O. bottae* by nuclear or mitogenomic data, respectively. (v) Moreover, *O. leucura* and *O. leucopyga* formed a sister clade to the *O. lugubris/lugentoides* clade according to the nuclear species tree, but mitogenomes placed them consecutively at the root of the clade including *O. finschi* and the *lugens* complex.

To understand whether nuclear gene trees were entirely discordant with mitogenomic relationships or in part reflected the latter, for each of the above discordances we checked for nuclear gene trees that agreed with the mitogenomic tree. This showed that for most of the mitonuclear discordances, roughly 15% of the gene trees agreed with the mitogenomic relationships (*picata* complex: 14.40%, 4,282 of 29,730 gene trees; *hispanica* complex: 13.13%, 3,905 of 29,730 gene trees; *isabellina* clade: 15.71%, 4,671 of 29,730 gene trees; *lugens* complex: 2.77%, 824 of 29,730 gene trees).

Time trees

In addition to the species' relationships, we were interested in understanding the time scales at which species diverged. Due to the lack of appropriate fossils, we resorted to first estimate a time-calibrated mitochondrial phylogeny based on the 13 mitochondrial protein-coding genes, for which substitution rates are available (Lerner et al. 2011). The analysis in BEAST 2.6.6 showed high convergence of all parameters in the three independent runs after 25% of the trees were discarded as burn-in (ESS >300). The results were in good agreement with pervious results obtained from single genes (Alaei Kakhki et al. 2016), dating the origin of open-habitat chats to the Miocene about 5.67 million years ago (mya) (95% highest posterior density (HPD): 5.32–6.06 mya). The diversification of wheatears (genus *Oenanthe*) started about 5.09 mya (95% HPD: 4.75–5.44 mya) **(Fig. 1, Fig. S3)**.

We then used the diversification time of the open-habitat chats estimated from mitochondrial data as a time constraint in dating analyses based on nuclear data. For these analyses, we first provided the topology and branch lengths obtained from ML analyses of concatenated BUSCO data along with 1.8 Mb high-confidence nuclear data (see Material and Methods) to generate the time-calibrated tree with RelTime-ML (Kumar et al. 2018). Compared to the mitochondrial results, the nuclear data mostly estimated similar divergence times between clades and shorter divergence times within clades (Pearson's r=0.93, p<0.001) (**Fig. 1, Fig. S3**). Second, we performed dating analyses for windowed loci across the genome the same way as for BUSCO by providing 3.8 Mb high-confidence data. Divergence times based on BUSCO strongly

correlated with ones estimated from windowed loci (Pearson's r=0.99, p<0.001) **(Fig. S4)**. A test in which we re-ran the estimation of mitochondrial divergence times in RelTime-ML the same way as for nuclear data yielded the same divergence times as estimated in BEAST, thus confirming that differences in divergence times between mitochondrial and nuclear data are not due to the approach but reflect the different data types.

Extensive Gene Tree Heterogeneity

Having established the species tree, we aimed to quantify the levels of gene tree heterogeneity in wheatears to understand whether the processes generating gene tree heterogeneity could potentially underly phenotypic parallelism in this core group of open-habitat chats that displays the highest incidence of phenotypic parallelism.

Several lines of evidence demonstrate extensive gene tree heterogeneity in wheatears. Remarkably, not a single gene tree out of 29,730 gene trees matched the species tree. Furthermore, many branches of the species tree – including ones with local posterior probability 1 – showed a high number of conflicting compared to concordant bipartitions, as evidenced by low Internode Certainty All (ICA) scores (**Fig. S5**), with ICA ranging from 1 to 0.35 and average ICA of 0.65 ± 0.19 (mean ± standard deviation). The high gene tree heterogeneities highlighted by ICA were further supported by low percentages of gene trees recovering the topology of the species tree at these internodes, as estimated by the gene concordance factor (gCF) (**Fig. 1**) that ranged from 1 to 0.06 with an average of 0.52 ± 0.30 (mean ± standard deviation). ICA and gCF were highly correlated (Pearson's r=0.94, p<0.001) **(Fig. S5)**. As expected, evidence for extensive gene tree heterogeneity was highest in clades with branches classified as within the phylogenetic anomaly zone. These included the *lugens*, *picata*, and *hispanica* complexes, the *isabellina* clade, and the placement of *O. leucopyga* and *O. leucura.*

Contributions of ILS to Gene Tree Heterogeneity

Next, we aimed to understand to which extent the levels of gene tree heterogeneity observed in wheatears can be explained by ILS alone. To this end, we first tested whether the MSC without hybridization adequately explains the gene tree heterogeneity observed across the entire species tree. The Tree Incongruence Checking in R (TICR) test (Stenz et al. 2015) showed an excess of outlier quartets ($p < 0.01$), indicating that a model including ILS but not introgression does not adequately explain the observed gene tree heterogeneity. This suggests that introgression occurred during the evolutionary history of wheatears.

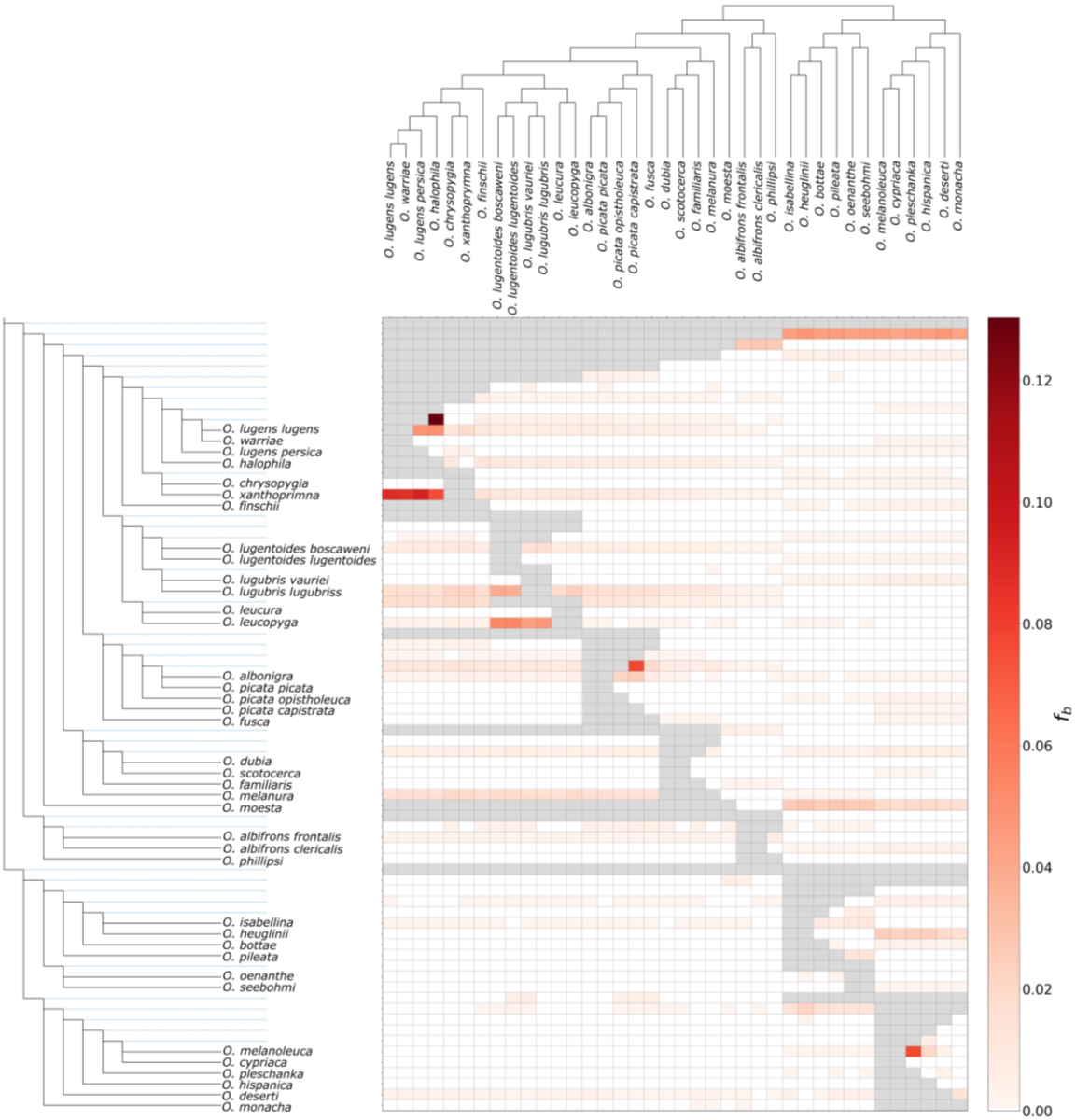

Figure 3 | Footprints of introgression as estimated by the f-branch statistic. The heat map summarizes the f-branch statistics estimated in Dsuite. Darker colors depict increasing evidence for gene flow between lineages. Dotted lines in the phylogeny represent ancestral lineage.

Therefore, we moved on to infer for each branch in the species tree separately whether ILS alone may explain the level of gene tree heterogeneity. To this end, for each internal branch, we estimated the number of gene trees supporting the first and second alternative topologies, based on the rationale that under ILS the first and second alternative gene tree topologies should be supported by an equal number of gene trees (Sayyari and Mirarab 2018). We identified 11 out of 37 internal branches (30%) for which the number of gene trees supporting the two alternative topologies were not significantly different (colored branches in **Fig. 1**). At these 11 internal branches, ILS alone can thus explain gene tree heterogeneity, while asymmetries at the other 26 internal branches may need to invoke other processes.

Contributions of Introgression to Gene Tree Heterogeneity

Given that gene tree heterogeneity at many branches could not be explained by ILS alone, we set out to infer footprints of introgression across wheatears. To this end, we first applied the approach based on D-statistics (Durand et al. 2011) implemented in Dsuite using > 58 million biallelic SNPs. This approach estimates D and f4 statistics across all possible combinations of trios in wheatears and then performs an f-branch test to assign gene flow to specific internal branches. The f-branch test suggested multiple events of introgression (**Fig. 3**):(i) *O. halophila* and the ancestor of *O. lugens lugens* and *O. warriae*, (ii) *O. xanthoprymna* and the ancestor of the *lugens* complex, (iii) *O. leucopyga* and the ancestor of the *O. lugubris/lugentoides* clade, (iv) *O. picata capistrata* and the ancestor of *O. picata picata* and *O. albonigra*, and (v) *O. melanoleuca* and *O. pleschanka*.

Finally, we corroborated the evidence for introgression in the *hispanica, lugens,* and *picata* complexes with MSC network analyses in phyloNet, allowing for 0-5 introgression events. According to the Bayesian Information Criterion (BIC), models involving reticulation events better fit the data than strictly bifurcating trees in all three complexes (**Tab. S2**). In the *lugens* complex, two introgression events were detected: between *O. xanthoprymna* and the ancestor of *O. lugens* (γ=49%), and between *O. halophila* and the *O. lugens lugens-O. warriae* ancestor (γ=25%) (**Fig. 4**). One introgression event was detected in the *picata* complex, between *O. picata capistrata* and the ancestor of *O. picata picata* and *O. albonigra* (γ=8%) (**Fig. 4**). In the *hispanica* complex, the highest scoring network involved two introgression edges: one between *O. melanoleuca* and *O. pleschanka* (γ=17%), and one between *O. hispanica* and the *O. cypriaca-melanoeuca* ancestor (γ=1%) (**Fig. 4**).

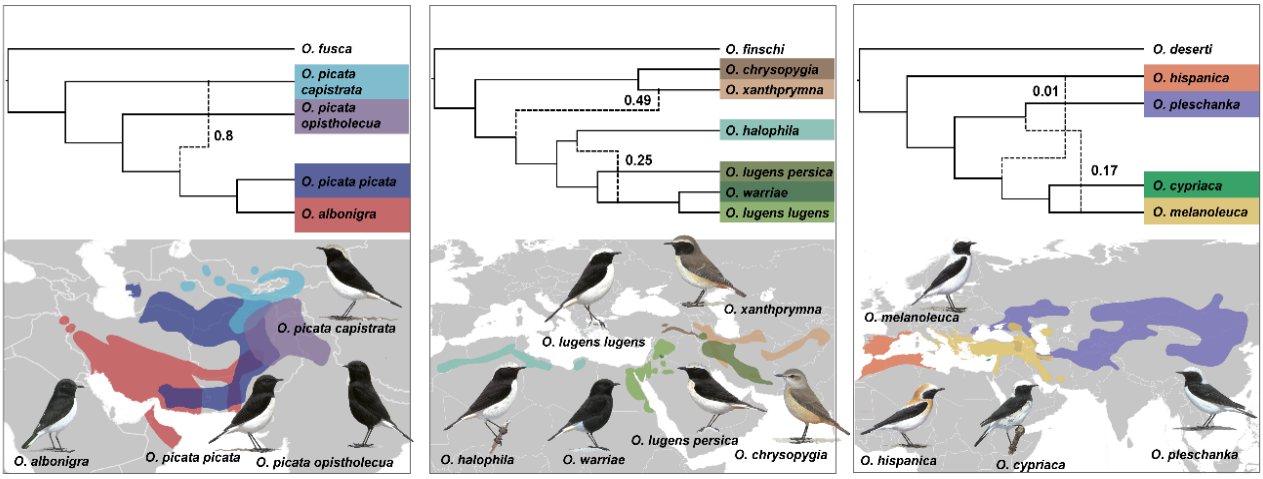

Figure 4 | Phylogenomic networks and distribution ranges for the *picata* (left), *lugens* (middle) and *hispanica* (right) complexes. Phylogenomic networks were estimated under the maximum pseudolikelihood approach implemented in phyloNet. Numbers on the edges indicate the inheritance probabilities, which correspond to the proportion of gene trees supporting the reticulate relationship. Drawings courtesy of Chris Rose (www.chrisrose-artist.co.uk) with permission from Bloomsbury Publishing Plc. Distribution ranges modified from BirdLife International and the Handbook of the Birds of the World (2016).

Discussion

The present study provides the first genomic insights into the speciation history of open-habitat chats and into the processes involved in shaping gene tree heterogeneity that may also underpin the high incidence of phenotypic parallelism in this group of songbirds. Our analyses reveal unambiguous species relationships despite considerable gene tree heterogeneity, including several mito-nuclear discordances that result from a combination of ILS and introgression. These relationships reconstructed from genomic data provides the strongest evidence yet for a high incidence of phenotypic parallelism in open-habitat chats, as exemplified for three phenotypes in **Fig. 1**.

We first discuss how mito-nuclear discordances and incidences of introgression together with known histories of hybridization and biogeographic history mold into a comprehensive picture of open-habitat chat evolution. We close by concluding based on the indirect evidence presented here that phenotypic parallelism in open habitat chats likely evolved through a combination of ILS, introgression and novel mutations in independent lineages. Together, our results paint a picture of genomic and phenotypic evolution that is in part marked by the sharing of ancestral variation and an exchange of genetic variation between species. Our study therefore contributes to the increasing body of evidence that phenotypic and species evolution not only proceed from novel mutations but abundantly reuse genetic variation present in ancestral and related species (Marques et al. 2019b; Meier et al. 2018; Seehausen et al. 2014).

Mito-nuclear discordances, patterns of introgression, hybridization history, and biography mold into a coherent picture of complex open-habitat chat evolution

The species relationships inferred from nuclear genomic data were in good agreement with previous phylogenies based predominantly on single mitochondrial markers (Aliabadian et al. 2012; Schweizer and Shirihai 2013) and thereby confirmed the biogeographic history of open-habitat chats (Alaei Kakhki et al. 2016). Still, we recovered several species relationships discordant between the nuclear genome and the mitogenome (Toews and Brelsford 2012). In the light of (i) the histories of introgression also uncovered here, (ii) the known hybridization history, and (iii) the here confirmed biogeography, most of these mito-nuclear discordances can be well embedded in a coherent history of open-habitat evolution.

The close nuclear relationship of *O. albonigra* with the nominate subspecies *O. p. picata* is in stark contrast with the mitochondrial divergence of *O. albonigra* with all *O. picata* subspecies about 0.5 mya (**Fig. 4a**). However, as an exception for wheatears, even from a perspective of plumage coloration the nuclear species tree implies a more parsimonious history of phenotypic evolution, as *O. albonigra* and *O. p. picata* display almost identical plumages. The high mitochondrial similarity of all subspecies currently treated under *O. picata* according to Panov

(2005) may be a result of introgressive hybridization. Indeed, the high abundance of admixed phenotypes in zones of contact between the members of this species complex (Panov 2005) suggests a high incidence of hybridization. Different from the *hispanica* complex, where taxa meet in restricted zones, lineages of the *picata* complex all mold together in a relatively large area in southern Central Asia, and their degree of reproductive isolation is largely unknown. Further population genomic insights are required from the *picata* complex to obtain detailed insights into its history of hybridization and phenotypic evolution.

The evolution of the *lugens* complex was marked by two incidences of introgression that likely underpin the mito-nuclear discordance observed in this complex (**Fig. 4b**). Introgression occurred between *O. xanthoprymna* and the *O. lugens* ancestor and between north-African *O. halophila* and the middle eastern *O. l. lugens-O. warriae* ancestor. Both incidences of introgression make sense in the light of biogeography, as they occurred between geographically neighboring taxa (**Fig. 4b**). Together they can explain the close mitochondrial relationship of *O. l. persica* with *O. xanthoprymna* and *O. chrysopygia*: *O. xanthoprymna* mitochondria were introduced into the *O. lugens* ancestor by introgression and may at first have segregated in the *O. lugens* lineage but then have been lost in *O. halophila.* Mitochondrial replacement with *O. halophila* variation upon genetic exchange of the latter taxon with the *O. l. lugens-O. warriae* ancestor would have left *O. l. persica* the only taxon with a *O. xanthoprymna*-like mitogenome. Importantly, our results shed first genomic light on the divergence of Basalt Wheatear (*O. warriae*), a species with a very restricted range that is interesting from the perspective of phenotypic evolution: this species turns out to be highly similar to *O. l. lugens* at the genomic level, which contrasts with its marked phenotypic divergence (**Fig. 4b**). This result is similar to the situation observed, for instance, in Hooded and Carrion Crows (*Corvus cornix* and *C. corone*, respectively) (Poelstra et al. 2014) and opens interesting questions on the evolutionary history of this taxon's coloration. Finally, in the *hispanica* complex, the incomplete sorting of mitochondrial variation was previously well documented (Alaei Kakhki et al. 2018; Randler et al. 2012), and footprints of introgression came as no surprise: The complex is characterized by pervasive hybridization of *O. melanoleuca* with *O. pleschanka* in several geographic regions (Haffer 1977; Panov 1992) and population genomic analyses suggest rates of introgression of up to almost 20% between these species (Schweizer et al. 2019a). Research is underway to uncover the detailed histories of hybridization in this Eurasian wheatear complex.

The thus far discussed mito-nuclear discordances were all accompanied with high levels of gene tree heterogeneity (most within the phylogenetic anomaly zone). However, most of these cases were not explained by ILS alone but went along with footprints of introgression. Still, part of the observed mito-nuclear discordances might well be a consequence of ILS. In the *picata* complex, for instance, lineage divergence occurred in rapid succession (**Fig. 1**), and ILS might well

be an alternative explanation for the mitochondrial divergence of the *O. albonigra* mitogenome. In addition, in the clade including *O. heuglinii* and the very widespread *O. isabellina*, species split in fast succession and the high levels of ILS likely explain the observed mito-nuclear discordance.

Taken together, our results demonstrate that the speciation history of open-habitat chats is similarly complex as their phenotypic evolution. Multiple events of introgression at both extant and ancestral time scales, along with abundant ILS, contributed to reticulate evolution and thus a mosaic of genomic variation in several clades of wheatears. Our study thus adds to an increasing number of examples (Enciso-Romero et al. 2017; Han et al. 2017; Lamichhaney et al. 2018; Meier et al. 2017) highlighting that species diversification is often complex and rather than by a linear process is at least in part a network of interacting lineages (Marques et al. 2019b)

Diverse routes to phenotypic parallelism in open-habitat chats

The reconstruction of relationships among open-habitat chats using genomic data has a deep impact on our understanding of phenotypic evolution in these songbirds: the species tree provides firm evidence for an extraordinary incidence of phenotypic parallelism (**Fig. 1**). For numerous traits, including plumage coloration, sexual dimorphism, and migration behavior, not related species display more similar phenotypes than sister species (**Fig. 1**). Almost entirely black plumages, for instance, evolved in five clades (*O. picata opistholeuca*, *O. warriae*, *O. leucura*, female *M. monticola*, and juvenile *O. leucopyga*), and sexually monomorphic female-type plumage is found in another five clades (*O. chrysopygia*, *O. fusca*, the *O. melanura* clade, the *O. isabellina* clade, and in the sub-Saharan clade), to name just two out of many examples.

Furthermore, our results suggest (directly for introgression and ILS, indirectly for parallel evolution *sensu stricto*) that phenotypic parallelism in open-habitat chats is unlikely explained by a single process but may need to invoke all possible routes (Hedrick 2013; Konečná et al. 2021; Montejo-Kovacevich et al. 2021; Natarajan et al. 2015; Pease et al. 2016), with the most likely processes depending on both demography and the phylogenetic scale.

For ILS to contribute to phenotypic parallelism, species must diverge in fast succession and maintain critically high effective population sizes to pass on ancestral variation and maintained it in daughter lineages. In open-habitat chats, such fast radiations occurred predominantly at rather recent timescales. The shortest split intervals are observed (in increasing order) in the *picata*, *hispanica*, and *lugens* complexes (**Fig. 1**). However, phenotypic parallelism of species in the *lugens* complex and of the *picata* complex is only found with other clades but not within the complexes. Given that the levels of ILS at the root of the *lugens* complex are restricted, ILS is unlikely to have contributed to phenotypic parallelism with other clades of wheatears sporting, for instance, similar plumages (see for instance the aforementioned example including *O. warriae*). Phenotypic parallelism is, however, observed for back and neck-side coloration in the *hispanica* complex (Schweizer et al. 2019a), and could be explained by ILS.

Likewise, introgression would need to involve taxa with similar phenotype to explain phenotypic parallelism. Our analyses indeed uncovered several instances of in part substantial introgression (**Fig. 3**, **Fig. 4**). However, despite suggesting that introgression provided the opportunity to exchange phenotypes between species, none of the inferred introgression events can be tied to concrete examples of phenotypic parallelism. This raises the question, whether the inferences of introgression applied here are underpowered to infer footprints of introgression relevant to phenotypic evolution of open-habitat chats, or whether, indeed, introgression played a limited role in these songbirds' phenotypic evolution.

Finally, many if not most phenotypic similarities in open-habitat chats are found across major phylogenetic clades that diverged around 5 mya (for instance the examples provided at the entry of the discussion). The split events at these time scales did not occur within short evolutionary time scales and, accordingly, levels of ILS are rather low for at least one of the relevant nodes (**Fig. 1**). Although gene tree heterogeneity was non-negligible for the larger of the two major wheatear clades, gene trees were mostly concordant for the root nodes of the wheatear clade including the *hispanica* complex and the *O. oenanthe* and *O. isabellina* clades (**Fig. 1**). Moreover, the phenotypically similar species occur in geographically well separated ranges and hybridization is thus rather unexpected. In conclusions, unless the approaches used here to detect the ILS and introgression are underpowered, the indirect evidence provided by our results suggests that many incidences of phenotypic parallelism at such timescale may have involved independent mutations to underpin the same phenotype, that is, parallel evolution *sensu stricto*.

Conclusion

In the present study we set out to probe gene tree variation for footprints of ILS and introgression with the goal of understanding how ILS and introgression may have contributed to phenotypic parallelism in open-habitat chats. Our results reveal a complex speciation history and provide conclusive evidence for abundant phenotypic parallelism in open-habitat chats. While we cannot conclude on the involvement of specific processes in the evolution of specific phenotypic parallelisms, the indirect evidence gained from the structure of the species tree and inferred levels of ILS and introgression suggest that the evolution of phenotypic parallelism in open-habitat chats likely occurred along all diverse trajectories, namely ILS, introgression, and parallel evolution through novel mutations. Thereby, our results contribute to a growing body of evidence that evolution makes use and re-use of all resources it has at hand including both standing (ancestral or heterospecific) as well as novel genetic variation.

481 # Material and Methods

482 ## Taxon sampling, DNA extraction, and whole-genome resequencing

483 Aiming for complete taxon sampling, we sequenced the genomes of 50 open-habitat chat taxa from
484 a total of 44 species from the genera *Oenanthe*, *Campicoloides, Emarginata*, *Myrmecocichla*,
485 *Pinarochroa*, and *Thamnolaea* (**Fig. 2**; **Tab. 1**). This sampling included all but three species (*E.*
486 *tractrac*, *M. collaris*, *T. coronata*) of the 47 currently recognized open-habitat chat species (Gill et
487 al. 2020). A genome sequence of *Saxicola maurus* (European Nucleotide Archive accession
488 number: ERR2560200-ERR2560209), a species of open-habitat chats' sister lineage (Sangster et
489 al. 2010; Zuccon and Ericson 2010), was included as an outgroup to root the open-habitat chat
490 species tree. We followed the taxonomy of the IOC World Bird List (v12.1) (Gill et al. 2020) except
491 for the *picata* complex, where we treat subspecies *picata, capistrata* and *opistholeuca* separately,
492 following Panov (2005).

493 We extracted DNA from blood stored in ≥96% ethanol or Queen's Lysis buffer or tissues
494 stored in 96% ethanol for taxa for which fresh material was available, or from toepads or dried
495 skin from skin-preparation sutures for taxa for which only museum samples were available (**Tab.**
496 **1**). From blood and tissue samples DNA was extracted using the DNeasy Blood and Tissue Kit
497 (Qiagen) or the MagAttract HMW DNA kit (Qiagen) following the manufacturer's protocol with
498 exception of an adapted digestion of blood samples as reported in Lutgen et al (Lutgen et al. 2020).
499 DNA from toepads and dried skin was extracted using the QIAamp DNA Micro Kit (Qiagen) with
500 an adapted digestion protocol that ensures high quantities of DNA
501 (dx.doi.org/10.17504/protocols.io.dm6gpwrdplzp/v1). DNA concentrations were quantified on a
502 Qubit fluorometer (dsDNA BR assay, Thermo Fisher Scientific) and DNA integrity was evaluated
503 on a TapeStation (MANUFACTURER, KIT). We prepared sequencing libraries using the ThruPLEX
504 DNA-Seq Kit (Takara), the Illumina DNA Prep Kit, the Illumina DNA PCR-free Kit, or the Chromium
505 Genome Library kit (10X Genomics) for intact DNA, or for fragmented DNA with the ACCEL-NGS
506 1S DNA Library Prep Kit (Swift Biosciences) (**Tab. 1**). All libraries were sequenced (150 bp paired-
507 end) on Illumina NovaSeq6000 instruments with a target coverage of ca. 15x.

508 ## Data preparation

509 *Adapter trimming and mapping of resequencing data*

510 Prior to further analysis, for all but the linked-read sequencing data, we trimmed adapters and
511 merged overlapping paired-end reads using fastp 0.20.0 (Chen et al. 2018). For linked-read
512 sequences, we trimmed the first 22 bp on the R1 read to eliminate the 10X indexes. We then
513 mapped the reads to the reference genome assembly of *Oenanthe melanoleuca* (Peona et al. in
514 prep.) using BWA 0.7.17 (Li 2013) and marked duplications with PicardTools 2.9.1
515 (http://broadinstitute.github.io/picard). After excluding duplicates, the average sequencing

516 coverage per individual ranged from 4.6x to 40.6x (mean and median 12.2, standard deviation
517 6.20) (**Tab. 1**).

518 *Base quality score recalibration (BQSR), SNP calling, and SNP genotyping*

519 Data preparation followed the GATK 4.1.4.1 (McKenna et al. 2010) best practices pipeline. First,
520 to prepare a list of high-confidence SNPs for BQSR, we ran HaplotypeCaller to generate gvcf files
521 for each sample and then merged gvcf files of all samples with CombineGVCFs before genotyping
522 SNPs using GenotypeGVCFs. To retain only high-confidence SNPs in the SNP-exclude set for BQSR,
523 we retained only SNPs that fulfilled the following criteria: mapping quality > 40, Fisher strand (FS)
524 phred-scaled p-value < 60, SNP quality score > 20, mapping quality rank sum value > -12.5, read
525 pos rank-sum test value > -8.0 and quality by depth > 2. We retained only biallelic SNPs with at
526 least one homozygous reference and one homozygous alternative genotype or with at least three
527 observations of reference and alternative alleles. We excluded the resulting set of SNPs from BQSR
528 in GATK. Following BQSR, we ran HaplotypeCaller on base-score-recalibrated bam files. The
529 resulting gvcf files of all samples where merged (CombineGVCFs) and variant and invariant sites
530 genotyped using the 'include-non-variant-sites' flag in GenotypeGVCFs. For all subsequent
531 analyses we based genotypes on genotype likelihoods. This resulted in 871,428,254 unfiltered
532 sites when the outgroup was included and 872,152,150 unfiltered sites without the outgroup.

533 In phylogenomic data sets, which are based on mapping of resequencing data to a
534 reference genome, data of species more divergent from the reference genome may risk mapping
535 at a lower percentage. To check for such mapping-related biases in our dataset, we estimated the
536 average number of nucleotide differences (d_{XY}) between *Oenanthe melanoleuca* (reference
537 genome) and all other species using pixy 0.95.02 (Korunes and Samuk 2021). We then estimated
538 the mapping percentage for all species using SAMtools (Li et al. 2009) and tested whether there
539 was a correlation between d_{XY} and mapping success.

540 *Data filtering*

541 Before data analysis, we removed all repeat regions from the multi-sample VCF file using the
542 repeat mask reported in Peona et al. (in prep.). Then we used BCFtools 1.11 (Li 2011) to remove
543 indels, sites close to indels (up to 10 bp) and all the sites at which exclusively alternative alleles
544 were called. For analyses requiring variant sites only, we removed all SNPs with more than 20%
545 missing data and all invariant sites using BCFtools and retained only SNPs with a minimum read
546 depth of five. To ensure linkage-disequilibrium (LD) among SNPs, we LD-pruned SNPs in VCFtools
547 0.1.16 (Danecek et al. 2011) such as to only retain SNPs with a minimum distance of 1 kb between
548 them. This physical distance is expected to remove most LD between SNPs, as e.g. in flycatchers
549 LD breaks down in most genomic regions after 1 kb (Ellegren et al. 2012). After this filtering, we
550 genotyped based on genotype likelihoods and retained 994,150 multiallelic SNPs. In addition, for

551 analyses that require biallelic SNPs exclusively, we removed all multiallelic SNPs from the VCF file
552 after the above filtering, using BCFtools.
553 For phylogenomic analyses requiring sequence data including both variant and invariant
554 sites, we defined 10 kb non-overlapping windows across the genome. Henceforth, we refer to the
555 windowed data as "loci" and to phylogenetic trees inferred therefrom as "gene trees". To make
556 sure that the adopted filtering strategy did not affect our results, we generated four sets of fasta
557 alignments using different filter settings for minimum read depth (DP), minimum percentage of
558 the window covered by data (PW), and missing data per site (MD) for both the 10 kb loci and the
559 BUSCO data set: (i) DP=1, PW=50%, MD=15%, (ii) DP=5, PW=50%, MD=15%, (iii) DP=1,
560 PW=50%, MD=5%, and (iv) DP=1, PW=80%, MD=10%. These four filtering strategies yielded the
561 same species tree and concatenated tree for 10 kb loci as well as for BUSCOs. For these analyses,
562 we therefore exclusively report the results based on the most stringent filtering on read depth (ii,
563 DP=5, PW=50%, MD=15%). For gene tree heterogeneity analyses, on the other hand, we aimed to
564 include the broadest representation of the genome and to this end retained all loci (N=29,730)
565 that fulfilled less stringent filtering criteria (i, DP=1, PW=50%, MD=15%).
566 Finally, for analyses making assumptions on intra- and inter-locus recombination (such as
567 species tree reconstructions) we made sure to include only loci with no intra-locus but free inter-
568 locus recombination. To this end, we excluded all loci with recombination signals ($P \leq 0.05$) as
569 inferred from the pairwise homoplasy index Phi (Φw) estimated in PhiPack 1.1 program (Bruen
570 et al. 2006). The criterion $P \leq 0.05$ does not account for multiple testing, but we preferred to
571 conservatively exclude loci with evidence for intra-locus recombination. To possibly retain only
572 loci among which free recombination occurs, we ensured a minimum distance of 10 kb by
573 including no two consecutive loci. At this distance, no LD occurs in flycatchers (Ellegren et al.
574 2012).

575 *Inference of Benchmarking Universal Single-Copy Ortholog (BUSCO) sequences*
576 Phylogenomic analyses based on the mapping of resequencing data to a reference genome,
577 especially when including species well diverged from the latter, may be affected by several biases.
578 For species more divergent from the reference genome, data from faster evolving genomic regions
579 (i) risks not being mapped, if these regions are too diverged from the reference sequence, or (ii)
580 may map to paralogs, if the species experienced different duplication histories (Chakrabarty et al.
581 2017; Fitz-Gibbon et al. 2017). These biases are expected to be least important in slowly evolving
582 regions of the genome, especially in BUSCOs, that are conserved and by definition present in single
583 copies in most species. To minimize mapping-related biases in our phylogenomic reconstructions,
584 especially on rooting and placements of the most divergent species, we therefore extracted the
585 intervals in which avian BUSCOs (aves_odb10) are situated in our reference genome using BUSCO
586 5.0.0 (Simão et al. 2015).

Phylogenomic reconstructions and multispecies coalescent analyses

BUSCO-based rooting of the open-habitat chat species tree

First, to establish the root within open-habitat chats, we applied both concatenation and multispecies coalescent-based methods on BUSCO sequences, including the outgroup. First, we used all BUSCOs (N=7,335) to estimate the maximum likelihood tree in IQ-TREE 2.1.2 (Minh et al. 2020b) based on the concatenated BUSCOs, using with one partition for each BUSCO and a GTR+I+G substitution model for all partitions (Abadi et al. 2019). One thousand bootstrap replicates were run using the ultrafast bootstrap approximation (Hoang et al. 2018). Second, we estimated the species tree under the multispecies coalescent using ASTRAL-III (Zhang et al. 2018) based on BUSCOs without recombination signals and free inter-locus recombination (N=2,091). To this end, we inferred BUSCOs' gene trees in IQ-TREE 2.1.2 using a GTR+I+G substitution model and one thousand ultrafast bootstrap approximations. To ensure that species tree inferences were not affected by inaccurately estimated gene trees (Zhang et al. 2018), we collapsed branches with bootstrap support inferior to 80% using Newick Utilities 1.6 (Junier and Zdobnov 2010). Reconstructing the species tree by including all BUSCOs not considering intra- and inter-locus recombination (N=7,335) did not affect the result.

Phylogenomic and multispecies coalescent analyses based on full evidence

To reconstruct the concatenated tree and species tree based on full evidence data, that is, data from the maximal possible fraction of the genome, and to study gene tree heterogeneity along the genome, we excluded the *Saxicola* outgroup. Instead, we rooted the trees with the clade that is the outgroup to all other open-habitat chats (sub-Saharan clade, **Fig. S1**). Excluding *Saxicola* ensured that analyses were not biased by mapping issues caused by this outgroup's divergence.

To estimate the concatenated tree using maximum likelihood in IQ-TREE 2.1.2 we used all loci with a GTR+I+G substitution model and 1,000 ultrafast bootstrap approximations. To estimate the species tree under the multispecies coalescent using ASTRAL-III, we at first estimated maximum likelihood gene trees using IQ-TREE 2.1.2 with a GTR+I+G substitution model and one thousand ultrafast bootstrap approximations. Based on these gene trees (pruned for within-locus recombination and assuring free recombination between loci), we inferred the species tree using ASTRAL-III. Because ASTRAL relies on accurately estimated gene trees, we collapsed branches with bootstrap support inferior to 80% using Newick Utilities 1.6.

To find regions of the species tree that represent "anomaly zones" where the frequency of one of the alternative quartets is higher than that of the topology in agreement the species tree, we estimated local quartet supports for the main topology and its two alternatives in ASTRAL-III (Degnan and Rosenberg 2006). We used the anomaly_finder.py script to search for anomaly zones in our species tree (Linkem et al. 2016). To test if the gene tree discordance could be explained by

622 polytomies instead of bifurcating nodes, we carried out a quartet-based polytomy test as
623 implemented in ASTRAL-III.
624 To see whether the SNP-based species tree could confirm the sequence-based species tree,
625 we used the unlinked multiallelic SNPs to the multispecies coalescent model implemented in
626 SVDQuartets (Chifman and Kubatko 2014) in PAUP* 4 (Swofford 2003). We ran this with 1000
627 bootstrap replicates and summarized the result in a 50% majority-rule consensus tree.

628 *Phylogenetic relationships of mitogenomes*
629 We were interested in whether previously inferred relationships based predominantly on single
630 mitochondrial genes (Alaei Kakhki et al. 2016; Aliabadian et al. 2012; Schweizer and Shirihai
631 2013) were supported by full mitogenomes and in how the mitogenomic relationships compare
632 to the ones inferred from nuclear loci. To this end, we extracted and assembled mitochondrial
633 genomes from the genomic data of all open-habitat chats using MitoFinder 1.2 (Allio et al. 2020).
634 We used the published Isabelline Wheatear (*Oenanthe isabellina*) mitochondrial genome as a
635 reference (Genbank accession number: NC_040290.1) and annotated the mitochondrial genome
636 using the annotation pipeline integrated in MitoFinder. Finally, we aligned the 13 mitochondrial
637 protein coding gene sequences using the automatic alignment strategy in MAFFT 7.471 (Katoh
638 and Standley 2013). We checked the alignments in AliView 1.26 (Larsson 2014) and removed stop
639 codons within the coding sequences or indels for downstream analyses. We determined the best
640 partition scheme using the Akaike information criterion (AIC) implemented in PartitionFinder
641 2.1.1 (Lanfear et al. 2017) and used the GTR+G+I model for all partitions. Then we constructed
642 the maximum-likelihood tree from the concatenated supermatrix of all 13 genes in IQ-TREE 2.1.2
643 using the ultrafast bootstrap approximations with 1,000 replicates.

644 **Dating analyses**
645 Beside species' relationships we were interested in estimating the divergence time in open-
646 habitat chats. Because there are no appropriate fossils for calibration, we first ran BEAST 2.6.6
647 (Bouckaert et al. 2019) for 13 mitochondrial protein coding genes to estimate a time-calibrated
648 mitochondrial phylogeny. We included the mitochondrial genome sequence of *Saxicola maurus*
649 (GenBank accession number: MN356403.1) as an outgroup in these analyses. Substitution models
650 were inferred during the MCMS analyses with bModelTest (Bouckaert and Drummond 2017)
651 implemented as a package in BEAST 2.6.6. Published substitution rates for each mitochondrial
652 gene (Lerner et al. 2011) were implemented as means of the clock rates in real space of lognormal
653 distribution with standard deviations of 0.005. We defined a Yule speciation process for the tree
654 prior and an uncorrelated lognormal relaxed clock model. Three independent MCMC chains were
655 run for 50 million generations, each with sampling every 5,000 generations. Effective sample sizes
656 for all parameters and appropriate numbers of burn-in generations were checked with Tracer 1.5

(Rambaut and Drummond 2009). The three independent runs were combined using LogCombiner 2.6.6 (Bouckaert et al. 2019). We used TreeAnnotator 2.6.6 (Bouckaert et al. 2019) to calculate a maximum clade credibility tree and the 95% highest posterior density (HPD) distributions of each estimated node.

We then used the divergence time of the sub-Saharan clade from wheatears estimated from mitochondrial data as time constraint in dating analyses based on nuclear data using RelTime-ML implemented in MEGA 11 (Tamura et al. 2021). For this analysis, we provided the topology with branch length estimated in IQtree2 based on concatenated BUSCOs data retained after the most stringent filtering (ii, DP=5, PW=50%, MD=15%), along with high-confidence BUSCO alignments. The latter consisted of BUSCO data filtered for DP=5, MD=5% and length of each BUSCO alignments longer than 1kb. We used the same filtering to get the 10 kb non-overlapping windows across the genome and used the concatenated tree retained after most stringent filtering (ii, DP=5, PW=50%, MD=15%) to repeat the analyses based on loci across the genome. To ensure that the differences in divergence times between mitochondrial and nuclear data were not due to the different dating approaches, we re-estimated the mitochondrial divergence times in RelTime-ML using the same approach as for the nuclear datasets.

Inference of gene tree variation, ILS, and introgression

Inference of the levels of gene tree variation

To investigate gene tree heterogeneity across the genome, we used gene trees inferred from less stringent filtering criteria (i, DP=1, PW=50%, MD=15%) as described above. To infer how many gene trees reflect the species tree topology, we used the script 'findCommonTrees.py' (Edelman et al. 2019). To characterize the levels of gene tree heterogeneity across open-habitat chats, we compared the gene trees to the species tree. Specifically, we estimated “internode certainty all” (ICA) and the “gene concordance factor” (gCF). ICA quantifies the amount of gene tree heterogeneity for each internode of the species tree by calculating the number of all most prevalent conflicting bipartitions. It takes values ranging from -1 to 1, with values around zero indicating strong conflict; values towards 1 indicate robust concordance of gene trees with the species tree in the bipartition of interest; and negative values indicate discordance between the bipartition of interest and one or more bipartitions with a higher frequency (Salichos et al. 2014). While ICA thus represents the degree of conflict on each node of a species tree, gCF better reflects the gene tree heterogeneity around each branch, and is the percentage of gene trees supporting the two alternative topologies for each branch (Minh et al. 2020a). We estimated ICA and gCF with PhyParts 0.0.1 (Smith et al. 2015) and IQ-TREE 2.1.2 respectively.

691 *Tests of an ILS model*

692 Next, we were interested in understanding whether ILS can sufficiently explain the level of gene
693 tree heterogeneity observed at the level of the whole species tree. To this end, we applied the Tree
694 Incongruence Checking in R (TICR) test (Stenz et al. 2015) implemented in the Phylolm R package.
695 This test evaluates whether the multispecies coalescent adequately explains gene tree
696 heterogeneity across the species tree with no hybridization edges. TICR requires posterior
697 distributions of gene tree topologies inferred through Bayesian inference of gene trees. Therefore,
698 we first estimated posterior distributions of individual gene trees with MrBayes 3.2.7 (Ronquist
699 et al. 2012). MrBayes analyses ran using three independent runs of 20 million generations each,
700 sampling every 20,000th generation using a GTR+I+G model. We estimated the length of burn-in
701 using Tracer 1.5 (Rambaut and Drummond 2009) to ensure that our sampling of the posterior
702 distribution had reached sufficient effective sample sizes (ESS > 200) for parameter estimation.
703 We then ran BUCKy (Ané et al. 2007; Larget et al. 2010) using the posterior distribution of gene
704 trees after discarding 25% as burn-in to estimate the concordance factors (CFs) for the three
705 possible splits of all quartets. The inferred CF values were then tested against those expected
706 under a coalescent model that takes ILS but not hybridization into account (chi-squared test).

707 We then tested for each branch in the species tree whether the gene tree heterogeneity
708 reflected in gCF can be sufficiently explained by a model incorporating ILS alone. Under ILS alone
709 – assuming sorting of variation occurs by random genetic drift – proportions of alternative gene
710 trees for a rooted triplet are expected to be approximately equal (Hibbins and Hahn 2022; Sayyari
711 and Mirarab 2018; Sayyari et al. 2018), and the concordant tree topology (the topology in
712 agreement with the species tree) should be at least as frequent as the two discordant topologies
713 (Hibbins and Hahn 2022; Sayyari et al. 2018). In contrast, introgression between non-sister taxa
714 results in asymmetric proportions of gene trees in the rooted triplet (Durand et al. 2012; Green et
715 al. 2010). Therefore, we performed a chi-square tests comparing the number of gene trees
716 supporting the two discordant topologies. Under ILS, these two alternative topologies are
717 expected to be equally frequent among gene trees (He et al. 2020). For all these analyses we
718 accounted for uncertainty in gene tree topologies by collapsing branches with bootstrap support
719 <80%.

720 *Inferring footprints of introgression*

721 To infer footprints of introgression across the entire species tree, we estimated Patterson's D
722 (Durand et al. 2011) and related statistics in Dsuite (Malinsky et al. 2021) based on 58,963,109
723 biallelic SNPs. D and f4 statistics were estimated across all possible combinations of trios in our
724 38 wheatear taxa. We used Dtrios to calculate the sums of three different patterns (BABA, BBAA
725 and, ABBA) and D and f4-ratio statistics for all 8,437 possible trios. Dsuite uses the standard block-
726 jackknife procedure to assess the significance of the D statistic. Due to the large number of D-

statistics comparisons and difficulties disentangling false positives that may arise due to ancient gene flow, we performed the f-branch test (fb) implemented in Dsuite to assign gene flow to specific internal branches on the species tree. Then we visualized the output using Dsuite's dtools.py script.

We then aimed to obtain further support for the footprints of introgression that were suggested in *lugens, picata* and *hispanica* complex by the above approach based on the D-statistics. To this end, for these three complexes, we estimated phylogenetic networks from maximum likelihood trees generated from BUSCOs using the pseudolikelihood (InferNetwork_MPL) (Yu and Nakhleh 2015) and likelihood (CalGTProb) (Yu et al. 2014) approaches implemented in phyloNet 3.6.9 (Than et al. 2008). Due to the high computational demands, analyses were run for each of the clades containing signals of introgression in earlier analyses separately, namely for the *lugens, picata* and *hispanica* complexes. Furthermore, we only included BUSCO loci that had data available for all taxa of the respective complex. Outgroup species for each complex were selected based on the species tree. Analyses included 7,323 rooted gene trees for the *lugens* complex, 7,310 rooted gene trees for the *picata* complex, and 7,335 rooted gene trees for the *hispanica* complex. For each complex, we allowed for one to five reticulation events, with the starting tree corresponding to the species tree topology (-s), 0.9 bootstrap threshold for gene trees (-b) and 1,000 iterations (-x). To ensure convergence, the network searches were repeated 10 times. Then we estimated the likelihood by fixing the topology of the focal clade for the species tree (without any reticulation) and for each of the five networks (with different numbers of introgression edges) and calculated their likelihood scores. We determined the optimal network by calculating the Bayesian Information Criterion (BIC) from the maximum likelihood scores, the number of gene trees, the number of branch length being estimated, plus the number of admixture edges in each model. We used the browser-based tree viewer IcyTree (Vaughan 2017) to visualize the estimated networks (Vaughan 2017).

Acknowledgements

We thank all the natural history museums and their staff who provided material for this study: namely the American Museum of Natural History, New York; Natural History Museum, Tring; Field Museum of Natural History, Chicago; Natural History Museum of Los Angeles County, Los Angeles; Museum of Vertebrate Zoology, UC Berkeley; Natural History Museum, University of Oslo; Naturhistoriska riksmuseet, Stockholm; Texas A&M University Biodiversity Research and Teaching Collections, Texas College Station; University of Washington Burke Museum;, Seattle, Yale Peabody Museum; Zoological Museum, Natural History Museum of Denmark, Copenhagen; Zoologisches Forschungsmuseum König, Bonn; and Martin Haase, Vogelwarte Hiddensee, Universität Greifswald. Further samples were provided by José Luis Copete, and Marc Illa. We are indebted to the sequencing facilities of NGI Sweden in Solna and to the NGS platform of the University of Berne and their respective staff for their excellent services and to Marta Burri for sequencing library preparations. Computations were performed at the High-Performance Computing Cluster EVE, a joint effort of the Helmholtz Centre for Environmental Research (UFZ) and the German Centre for Integrative Biodiversity Research (iDiv) Halle-Jena-Leipzig. We thank the administration and support staff of EVE, Thomas Schnicke and Ben Langenberg (UFZ), and Christian Krause (iDiv). We thank Chris Rose and Claire Weatherhead from Bloomsbury Publishing Plc for their permission to use bird drawings in our figures. This research was supported by a German Research Foundation (DFG) research grant (BU3456/3-1) to RB, the National Research Fund (FNR), Luxembourg, grant number 14575729 to DL, and a Georg Foster Research Stipend of the Alexander von Humboldt Foundation and a scholarship for female researchers from Friedrich-Schiller-University Jena, both to NAK.

References

Abadi S, Azouri D, Pupko T, Mayrose I. 2019. Model selection may not be a mandatory step for phylogeny reconstruction. Nature communications. 10(1):1-11.

Alaei Kakhki N, Aliabadian M, Förschler MI, Ghasempouri SM, Kiabi BH, Verde Arregoitia LD, Schweizer M. 2018. Phylogeography of the oenanthe hispanica–pleschanka–cypriaca complex (aves, muscicapidae: Saxicolinae): Diversification history of open-habitat specialists based on climate niche models, genetic data, and morphometric data. Journal of Zoological Systematics and Evolutionary Research. 56(3):408-427.

Alaei Kakhki N, Aliabadian M, Schweizer M. 2016. Out of africa: Biogeographic history of the open-habitat chats (aves, muscicapidae: Saxicolinae) across arid areas of the old world. Zoologica Scripta. 45(3):237-251.

Aliabadian M, Kaboli M, Förschler MI, Nijman V, Chamani A, Tillier A, Prodon R, Pasquet E, Ericson PG, Zuccon D. 2012. Erratum to: Convergent evolution of morphological and ecological traits in the open-habitat chat complex (aves, muscicapidae: Saxicolinae). Molecular Phylogenetics Evolution. 65(3):35-45.

Allio R, Schomaker-Bastos A, Romiguier J, Prosdocimi F, Nabholz B, Delsuc F. 2020. Mitofinder: Efficient automated large-scale extraction of mitogenomic data in target enrichment phylogenomics. Molecular ecology resources. 20(4):892-905.

Ané C, Larget B, Baum DA, Smith SD, Rokas A. 2007. Bayesian estimation of concordance among gene trees. Molecular biology and evolution. 24(2):412-426.

Arendt J, Reznick D. 2008. Convergence and parallelism reconsidered: What have we learned about the genetics of adaptation? Trends in ecology & evolution. 23(1):26-32.

Barrett RD, Schluter D. 2008. Adaptation from standing genetic variation. Trends in ecology & evolution. 23(1):38-44.

Besnard G, Muasya AM, Russier F, Roalson EH, Salamin N, Christin P-A. 2009. Phylogenomics of c4 photosynthesis in sedges (cyperaceae): Multiple appearances and genetic convergence. Molecular Biology and Evolution. 26(8):1909-1919.

BirdLife International and Handbook of the Birds of the World (2016). Bird species distribution maps of the world. Version 6.0.

Bouckaert R, Vaughan TG, Barido-Sottani J, Duchêne S, Fourment M, Gavryushkina A, Heled J, Jones G, Kühnert D, De Maio N. 2019. Beast 2.5: An advanced software platform for bayesian evolutionary analysis. PLoS computational biology. 15(4):e1006650.

Bouckaert RR, Drummond AJ. 2017. Bmodeltest: Bayesian phylogenetic site model averaging and model comparison. BMC evolutionary biology. 17(1):1-11.

Bruen TC, Philippe H, Bryant D. 2006. A simple and robust statistical test for detecting the presence of recombination. Genetics. 172(4):2665-2681.

Brusatte SL, O'Connor JK, Jarvis ED. 2015. The origin and diversification of birds. Current Biology. 25(19):R888-R898.

Campagna L, Repenning M, Silveira LF, Fontana CS, Tubaro PL, Lovette IJ. 2017. Repeated divergent selection on pigmentation genes in a rapid finch radiation. Science advances. 3(5):e1602404.

Chakrabarty P, Faircloth BC, Alda F, Ludt WB, Mcmahan CD, Near TJ, Dornburg A, Albert JS, Arroyave J, Stiassny ML. 2017. Phylogenomic systematics of ostariophysan fishes: Ultraconserved elements support the surprising non-monophyly of characiformes. Systematic Biology. 66(6):881-895.

Chen S, Zhou Y, Chen Y, Gu JJB. 2018. Fastp: An ultra-fast all-in-one fastq preprocessor. 34(17):i884-i890.

Chifman J, Kubatko L. 2014. Quartet inference from snp data under the coalescent model. Bioinformatics. 30(23):3317-3324.

Chou J, Gupta A, Yaduvanshi S, Davidson R, Nute M, Mirarab S, Warnow T. 2015. A comparative study of svdquartets and other coalescent-based species tree estimation methods. BMC genomics. 16(10):1-11.

Christin P-A, Salamin N, Savolainen V, Duvall MR, Besnard G. 2007. C4 photosynthesis evolved in grasses via parallel adaptive genetic changes. Current biology. 17(14):1241-1247.

Christin P-A, Weinreich DM, Besnard G. 2010. Causes and evolutionary significance of genetic convergence. Trends in Genetics. 26(9):400-405.

Colosimo PF, Hosemann KE, Balabhadra S, Villarreal G, Dickson M, Grimwood J, Schmutz J, Myers RM, Schluter D, Kingsley DM. 2005. Widespread parallel evolution in sticklebacks by repeated fixation of ectodysplasin alleles. Science. 307(5717):1928-1933.

Cresko WA, Amores A, Wilson C, Murphy J, Currey M, Phillips P, Bell MA, Kimmel CB, Postlethwait JH. 2004. Parallel genetic basis for repeated evolution of armor loss in alaskan threespine

stickleback populations. Proceedings of the National Academy of Sciences. 101(16):6050-6055.

Danecek P, Auton A, Abecasis G, Albers CA, Banks E, DePristo MA, Handsaker RE, Lunter G, Marth GT, Sherry ST. 2011. The variant call format and vcftools. Bioinformatics. 27(15):2156-2158.

Degnan JH, Rosenberg NA. 2006. Discordance of species trees with their most likely gene trees. PLoS genetics. 2(5):e68.

Doyle JJ. 1997. Trees within trees: Genes and species, molecules and morphology. Systematic Biology. 46(3):537-553.

Durand EY, Patterson N, Reich D, Slatkin M. 2011. Testing for ancient admixture between closely related populations. Molecular biology and evolution. 28(8):2239-2252.

Durand S, Bouché N, Strand EP, Loudet O, Camilleri C. 2012. Rapid establishment of genetic incompatibility through natural epigenetic variation. Current Biology. 22(4):326-331.

Edelman NB, Frandsen PB, Miyagi M, Clavijo B, Davey J, Dikow RB, García-Accinelli G, Van Belleghem SM, Patterson N, Neafsey DE. 2019. Genomic architecture and introgression shape a butterfly radiation. Science. 366(6465):594-599.

Ellegren H, Smeds L, Burri R, Olason PI, Backström N, Kawakami T, Künstner A, Mäkinen H, Nadachowska-Brzyska K, Qvarnström A. 2012. The genomic landscape of species divergence in ficedula flycatchers. Nature. 491(7426):756-760.

Elmer KR, Meyer A. 2011. Adaptation in the age of ecological genomics: Insights from parallelism and convergence. Trends in ecology & evolution. 26(6):298-306.

Enciso-Romero J, Pardo-Díaz C, Martin SH, Arias CF, Linares M, McMillan WO, Jiggins CD, Salazar C. 2017. Evolution of novel mimicry rings facilitated by adaptive introgression in tropical butterflies. Molecular ecology. 26(19):5160-5172.

Eyre-Walker A, Keightley PD. 2007. The distribution of fitness effects of new mutations. Nature Reviews Genetics. 8(8):610-618.

Fitz-Gibbon S, Hipp AL, Pham KK, Manos PS, Sork VL. 2017. Phylogenomic inferences from reference-mapped and de novo assembled short-read sequence data using radseq sequencing of california white oaks (quercus section quercus). Genome. 60(9):743-755.

Funk DJ, Omland KE. 2003. Species-level paraphyly and polyphyly: Frequency, causes, and consequences, with insights from animal mitochondrial DNA. Annual Review of Ecology, Evolution, and Systematics. 34(1):397-423.

Genner MJ, Turner GF. 2012. Ancient hybridization and phenotypic novelty within lake malawi's cichlid fish radiation. Molecular Biology and Evolution. 29(1):195-206.

Gill F, Donsker D, Rasmussen P. 2020. Ioc world bird list (v10. 1). IOC World Bird List [consultado el 26 de julio de 2020] DOI: https://doi org/1014344/IOC ML. 10.

Gompel N, Prud'homme B. 2009. The causes of repeated genetic evolution. Developmental biology. 332(1):36-47.

Grant PR, Grant BR, Petren K. 2005. Hybridization in the recent past. The American Naturalist. 166(1):56-67.

Green RE, Krause J, Briggs AW, Maricic T, Stenzel U, Kircher M, Patterson N, Li H, Zhai W, Fritz MH-Y. 2010. A draft sequence of the neandertal genome. Science. 328(5979):710-722.

Gross JB, Borowsky R, Tabin CJ. 2009. A novel role for mc1r in the parallel evolution of depigmentation in independent populations of the cavefish astyanax mexicanus. PLoS genetics. 5(1):e1000326.

Haffer J. 1977. Secondary contact zones of birds in northern iran. Bonner Zoologische Monographien. 10:1-64.

Han F, Lamichhaney S, Grant BR, Grant PR, Andersson L, Webster MT. 2017. Gene flow, ancient polymorphism, and ecological adaptation shape the genomic landscape of divergence among darwin's finches. Genome research. 27(6):1004-1015.

He C, Liang D, Zhang P. 2020. Asymmetric distribution of gene trees can arise under purifying selection if differences in population size exist. Molecular biology and evolution. 37(3):881-892.

Hedrick PW. 2013. Adaptive introgression in animals: Examples and comparison to new mutation and standing variation as sources of adaptive variation. Molecular ecology. 22(18):4606-4618.

Heliconius Genome Consortium. 2012. Butterfly genome reveals promiscuous exchange of mimicry adaptations among species. Nature. 487:94-98.

Hermisson J, Pennings PS. 2005. Soft sweeps: Molecular population genetics of adaptation from standing genetic variation. Genetics. 169(4):2335-2352.

Hibbins MS, Hahn MW. 2022. Phylogenomic approaches to detecting and characterizing introgression. Genetics. 220(2):iyab173.

Hoang DT, Chernomor O, Von Haeseler A, Minh BQ, Vinh LS. 2018. Ufboot2: Improving the ultrafast bootstrap approximation. Molecular biology and evolution. 35(2):518-522.

Hoballah ME, Gübitz T, Stuurman J, Broger L, Barone M, Mandel T, Dell'Olivo A, Arnold M, Kuhlemeier C. 2007. Single gene–mediated shift in pollinator attraction in petunia. The Plant Cell. 19(3):779-790.

Hobolth A, Dutheil JY, Hawks J, Schierup MH, Mailund T. 2011. Incomplete lineage sorting patterns among human, chimpanzee, and orangutan suggest recent orangutan speciation and widespread selection. Genome research. 21(3):349-356.

Jarvis ED, Mirarab S, Aberer AJ, Li B, Houde P, Li C, Ho SY, Faircloth BC, Nabholz B, Howard JT. 2014. Whole-genome analyses resolve early branches in the tree of life of modern birds. Science. 346(6215):1320-1331.

Jones FC, Grabherr MG, Chan YF, Russell P, Mauceli E, Johnson J, Swofford R, Pirun M, Zody MC, White S. 2012. The genomic basis of adaptive evolution in threespine sticklebacks. Nature. 484(7392):55-61.

Junier T, Zdobnov EM. 2010. The newick utilities: High-throughput phylogenetic tree processing in the unix shell. Bioinformatics. 26(13):1669-1670.

Katoh K, Standley DM. 2013. Mafft multiple sequence alignment software version 7: Improvements in performance and usability. Molecular biology and evolution. 30(4):772-780.

Konečná V, Bray S, Vlček J, Bohutínská M, Požárová D, Choudhury RR, Bollmann-Giolai A, Flis P, Salt DE, Parisod C. 2021. Parallel adaptation in autopolyploid arabidopsis arenosa is dominated by repeated recruitment of shared alleles. Nature communications. 12(1):1-13.

Korunes KL, Samuk K. 2021. Pixy: Unbiased estimation of nucleotide diversity and divergence in the presence of missing data. Molecular ecology resources. 21(4):1359-1368.

Kumar S, Stecher G, Li M, Knyaz C, Tamura K. 2018. Mega x: Molecular evolutionary genetics analysis across computing platforms. Molecular biology and evolution. 35(6):1547.

Lamers RP, Muthukrishnan G, Castoe TA, Tafur S, Cole AM, Parkinson CL. 2012. Phylogenetic relationships among staphylococcus species and refinement of cluster groups based on multilocus data. BMC evolutionary biology. 12(1):1-15.

Lamichhaney S, Han F, Webster MT, Andersson L, Grant BR, Grant PR. 2018. Rapid hybrid speciation in darwin's finches. Science. 359(6372):224-228.

Lanfear R, Frandsen PB, Wright AM, Senfeld T, Calcott B. 2017. Partitionfinder 2: New methods for selecting partitioned models of evolution for molecular and morphological phylogenetic analyses. Molecular biology and evolution. 34(3):772-773.

Larget BR, Kotha SK, Dewey CN, Ané C. 2010. Bucky: Gene tree/species tree reconciliation with bayesian concordance analysis. Bioinformatics. 26(22):2910-2911.

Larsson A. 2014. Aliview: A fast and lightweight alignment viewer and editor for large datasets. Bioinformatics. 30(22):3276-3278.

Lerner HR, Meyer M, James HF, Hofreiter M, Fleischer RC. 2011. Multilocus resolution of phylogeny and timescale in the extant adaptive radiation of hawaiian honeycreepers. Current Biology. 21(21):1838-1844.

Li H. 2011. A statistical framework for snp calling, mutation discovery, association mapping and population genetical parameter estimation from sequencing data. Bioinformatics. 27(21):2987-2993.

Li H. 2013. Aligning sequence reads, clone sequences and assembly contigs with bwa-mem. arXiv preprint arXiv:13033997.

Li H, Handsaker B, Wysoker A, Fennell T, Ruan J, Homer N, Marth G, Abecasis G, Durbin R. 2009. The sequence alignment/map format and samtools. Bioinformatics. 25(16):2078-2079.

Linkem CW, Minin VN, Leaché AD. 2016. Detecting the anomaly zone in species trees and evidence for a misleading signal in higher-level skink phylogeny (squamata: Scincidae). Systematic biology. 65(3):465-477.

Lutgen D, Ritter R, Olsen RA, Schielzeth H, Gruselius J, Ewels P, García JT, Shirihai H, Schweizer M, Suh A. 2020. Linked-read sequencing enables haplotype-resolved resequencing at population scale. Molecular Ecology Resources. 20(5):1311-1322.

Maddison WP. 1997. Gene trees in species trees. Systematic biology. 46(3):523-536.

Malinsky M, Matschiner M, Svardal H. 2021. Dsuite-fast d-statistics and related admixture evidence from vcf files. Molecular Ecology Resources. 21(2):584-595.

Malinsky M, Svardal H, Tyers AM, Miska EA, Genner MJ, Turner GF, Durbin R. 2018. Whole-genome sequences of malawi cichlids reveal multiple radiations interconnected by gene flow. Nature ecology & evolution. 2(12):1940-1955.

Marques DA, Lucek K, Sousa VC, Excoffier L, Seehausen O. 2019a. Admixture between old lineages facilitated contemporary ecological speciation in lake constance stickleback. Nature communications. 10(1):1-14.

Marques DA, Meier JI, Seehausen O. 2019b. A combinatorial view on speciation and adaptive radiation. Trends in ecology & evolution. 34(6):531-544.

Martin A, Orgogozo V. 2013. The loci of repeated evolution: A catalog of genetic hotspots of phenotypic variation. Evolution. 67(5):1235-1250.

Mayr E, Stresemann E. 1950. Polymorphism in the chat genus oenanthe (aves). Evolution. 4:291-300.

McKenna A, Hanna M, Banks E, Sivachenko A, Cibulskis K, Kernytsky A, Garimella K, Altshuler D, Gabriel S, Daly M. 2010. The genome analysis toolkit: A mapreduce framework for analyzing next-generation DNA sequencing data. Genome research. 20(9):1297-1303.

Meier JI, Marques DA, Mwaiko S, Wagner CE, Excoffier L, Seehausen O. 2017. Ancient hybridization fuels rapid cichlid fish adaptive radiations. Nature communications. 8(1):1-11.

Meier JI, Marques DA, Wagner CE, Excoffier L, Seehausen O. 2018. Genomics of parallel ecological speciation in lake victoria cichlids. Molecular biology and evolution. 35(6):1489-1506.

Minh BQ, Hahn MW, Lanfear R. 2020a. New methods to calculate concordance factors for phylogenomic datasets. Molecular biology and evolution. 37(9):2727-2733.

Minh BQ, Schmidt HA, Chernomor O, Schrempf D, Woodhams MD, Von Haeseler A, Lanfear R. 2020b. Iq-tree 2: New models and efficient methods for phylogenetic inference in the genomic era. Molecular biology and evolution. 37(5):1530-1534.

Montejo-Kovacevich G, Meier JI, Bacquet CN, Warren IA, Chan YF, Kucka M, Salazar C, Rueda N, Montgomery SH, McMillan WO. 2021. Repeated genetic adaptation to high altitude in two tropical butterflies. bioRxiv.

Natarajan C, Projecto-Garcia J, Moriyama H, Weber RE, Muñoz-Fuentes V, Green AJ, Kopuchian C, Tubaro PL, Alza L, Bulgarella M. 2015. Convergent evolution of hemoglobin function in high-altitude andean waterfowl involves limited parallelism at the molecular sequence level. PLoS genetics. 11(12):e1005681.

Nater A, Burri R, Kawakami T, Smeds L, Ellegren H. 2015. Resolving evolutionary relationships in closely related species with whole-genome sequencing data. Systematic Biology. 64(6):1000-1017.

Outlaw RK, Voelker G, Bowie RC. 2010. Shall we chat? Evolutionary relationships in the genus cercomela (muscicapidae) and its relation to oenanthe reveals extensive polyphyly among chats distributed in africa, india and the palearctic. Molecular Phylogenetics and Evolution. 55(1):284-292.

Panov E. 1992. Emergence of hybridogenous polymorphism in the oenanthe picata complex. Bulletin of the British Ornithologists' Club Centenary Volume. 112:237-249.

Panov EN. 2005. Wheatears of palearctic. Pensoft.

Pardo-Diaz C, Salazar C, Baxter SW, Merot C, Figueiredo-Ready W, Joron M, McMillan WO, Jiggins CD. 2012. Adaptive introgression across species boundaries in heliconius butterflies. PLoS Genet. 8(6):e1002752.

Paterson RS, Rybczynski N, Kohno N, Maddin HC. 2020. A total evidence phylogenetic analysis of pinniped phylogeny and the possibility of parallel evolution within a monophyletic framework. Frontiers in Ecology and Evolution. 7:457.

Pease JB, Haak DC, Hahn MW, Moyle LC. 2016. Phylogenomics reveals three sources of adaptive variation during a rapid radiation. PLoS biology. 14(2):e1002379.

Peona V, Palacios-Gimenes O, Lutgen D, Olsen R, Alaei Kakhki N, Andriopoulos P, Bontzorlos V, Schweizer M, Suh A, Burri R. in prep. A chromosome-scale reference genome for eastern black-eared wheatear (oenanthe melanoleuca).

Poelstra JW, Vijay N, Bossu CM, Lantz H, Ryll B, Müller I, Baglione V, Unneberg P, Wikelski M, Grabherr MG. 2014. The genomic landscape underlying phenotypic integrity in the face of gene flow in crows. Science. 344(6190):1410-1414.

Preston JC, Hileman LC. 2009. Developmental genetics of floral symmetry evolution. Trends in plant science. 14(3):147-154.

Protas ME, Hersey C, Kochanek D, Zhou Y, Wilkens H, Jeffery WR, Zon LI, Borowsky R, Tabin CJ. 2006. Genetic analysis of cavefish reveals molecular convergence in the evolution of albinism. Nature genetics. 38(1):107-111.

Rambaut A, Drummond A. 2009. Tracer v1. 5.0. Available at: Http://beast.Bio.Ed.Ac.Uk/tracer.

Randler C, Förschler MI, Gonzalez J, Aliabadian M, Bairlein F, Wink M. 2012. Phylogeography, pre-zygotic isolation and taxonomic status in the endemic cyprus wheatear oenanthe cypriaca. Journal of Ornithology. 153(2):303-312.

Ronquist F, Teslenko M, Van Der Mark P, Ayres DL, Darling A, Höhna S, Larget B, Liu L, Suchard MA, Huelsenbeck JP. 2012. Mrbayes 3.2: Efficient bayesian phylogenetic inference and model choice across a large model space. Systematic biology. 61(3):539-542.

Salichos L, Stamatakis A, Rokas A. 2014. Novel information theory-based measures for quantifying incongruence among phylogenetic trees. Molecular biology and evolution. 31(5):1261-1271.

Sangster G, Alström P, Forsmark E, Olsson U. 2010. Multi-locus phylogenetic analysis of old world chats and flycatchers reveals extensive paraphyly at family, subfamily and genus level (aves: Muscicapidae). Molecular Phylogenetics and Evolution. 57(1):380-392.

Sayyari E, Mirarab S. 2018. Testing for polytomies in phylogenetic species trees using quartet frequencies. Genes. 9(3):132.

Sayyari E, Whitfield JB, Mirarab S. 2018. Discovista: Interpretable visualizations of gene tree discordance. Molecular Phylogenetics and Evolution. 122:110-115.

Schweizer M, Shirihai H. 2013. Phylogeny of the oenanthe lugens complex (aves, muscicapidae: Saxicolinae): Paraphyly of a morphologically cohesive group within a recent radiation of open-habitat chats. Molecular Phylogenetics Evolution. 69(3):450-461.

Schweizer M, Warmuth V, Alaei Kakhki N, Aliabadian M, Förschler M, Shirihai H, Suh A, Burri R. 2019a. Parallel plumage colour evolution and introgressive hybridization in wheatears. Journal of evolutionary biology. 32(1):100-110.

Schweizer M, Warmuth VM, Kakhki NA, Aliabadian M, Förschler M, Shirihai H, Ewels P, Gruselius J, Olsen R-A, Schielzeth H et al. 2019b. Genome-wide evidence supports mitochondrial relationships and pervasive parallel phenotypic evolution in open-habitat chats. Molecular phylogenetics evolution. 139:106568.

Seehausen O, Butlin RK, Keller I, Wagner CE, Boughman JW, Hohenlohe PA, Peichel CL, Saetre G-P, Bank C, Brännström Å. 2014. Genomics and the origin of species. Nature Reviews Genetics. 15(3):176-192.

Simão FA, Waterhouse RM, Ioannidis P, Kriventseva EV, Zdobnov EM. 2015. Busco: Assessing genome assembly and annotation completeness with single-copy orthologs. Bioinformatics. 31(19):3210-3212.

Smith SA, Moore MJ, Brown JW, Yang Y. 2015. Analysis of phylogenomic datasets reveals conflict, concordance, and gene duplications with examples from animals and plants. BMC evolutionary biology. 15(1):1-15.

Song Y, Endepols S, Klemann N, Richter D, Matuschka F-R, Shih C-H, Nachman MW, Kohn MH. 2011. Adaptive introgression of anticoagulant rodent poison resistance by hybridization between old world mice. Current Biology. 21(15):1296-1301.

Stahl BA, Gross JB. 2015. Alterations in mc1r gene expression are associated with regressive pigmentation in astyanax cavefish. Development genes and evolution. 225(6):367-375.

Stenz NW, Larget B, Baum DA, Ané C. 2015. Exploring tree-like and non-tree-like patterns using genome sequences: An example using the inbreeding plant species arabidopsis thaliana (l.) heynh. Systematic Biology. 64(5):809-823.

Stern DL. 2013. The genetic causes of convergent evolution. Nature Reviews Genetics. 14(11):751-764.

Stryjewski KF, Sorenson MD. 2017. Mosaic genome evolution in a recent and rapid avian radiation. Nature Ecology & Evolution. 1(12):1912-1922.

Suh A. 2016. The phylogenomic forest of bird trees contains a hard polytomy at the root of neoaves. Zoologica Scripta. 45:50-62.

Suh A, Smeds L, Ellegren H. 2015. The dynamics of incomplete lineage sorting across the ancient adaptive radiation of neoavian birds. PLoS Biol. 13(8):e1002224.

Swofford D. 2003. Paup*. Phylogenetic analysis using parsimony (*and other methods). Version 4 Sinauer Associates, Sunderland, Massachusetts.

Tamura K, Stecher G, Kumar S. 2021. Mega11: Molecular evolutionary genetics analysis version 11. Molecular biology and evolution. 38(7):3022-3027.

Than C, Ruths D, Nakhleh L. 2008. Phylonet: A software package for analyzing and reconstructing reticulate evolutionary relationships. BMC bioinformatics. 9(1):1-16.

Toews DP, Brelsford A. 2012. The biogeography of mitochondrial and nuclear discordance in animals. Molecular ecology. 21(16):3907-3930.

Van Belleghem SM, Vangestel C, De Wolf K, De Corte Z, Möst M, Rastas P, De Meester L, Hendrickx F. 2018. Evolution at two time frames: Polymorphisms from an ancient singular divergence event fuel contemporary parallel evolution. PLoS genetics. 14(11):e1007796.

Wallbank RW, Baxter SW, Pardo-Diaz C, Hanly JJ, Martin SH, Mallet J, Dasmahapatra KK, Salazar C, Joron M, Nadeau N. 2016. Evolutionary novelty in a butterfly wing pattern through enhancer shuffling. PLoS biology. 14(1):e1002353.

Whittall JB, Voelckel C, Kliebenstein DJ, Hodges SA. 2006. Convergence, constraint and the role of gene expression during adaptive radiation: Floral anthocyanins in aquilegia. Molecular Ecology. 15(14):4645-4657.

Wu M, Kostyun JL, Hahn MW, Moyle LC. 2018. Dissecting the basis of novel trait evolution in a radiation with widespread phylogenetic discordance. Molecular Ecology. 27(16):3301-3316.

Yu Y, Dong J, Liu KJ, Nakhleh L. 2014. Maximum likelihood inference of reticulate evolutionary histories. Proceedings of the National Academy of Sciences. 111(46):16448-16453.

Yu Y, Nakhleh L. 2015. A maximum pseudo-likelihood approach for phylogenetic networks. BMC genomics. 16(10):1-10.

Zhang C, Rabiee M, Sayyari E, Mirarab S. 2018. Astral-iii: Polynomial time species tree reconstruction from partially resolved gene trees. BMC bioinformatics. 19(6):15-30.

Zuccon D, Ericson PG. 2010. A multi-gene phylogeny disentangles the chat-flycatcher complex (aves: Muscicapidae). Zoologica Scripta. 39(3):213-224.

1098 **Table 1 | Sampling and sequence data information**.
1099

Taxon	Collection, no.[a]	Tissue	Library Type	Mapping %	Coverage
Campicoloides bifasciatus	MVZ, RSA073,	Muscle	Illumina DNA Prep Kit	99.1	8.5
Emarginata schlegelii	FMNH, 453197,	Muscle	Illumina DNA Prep Kit	99.1	9.5
Emarginata sinuata	UWMB, 95470	Muscle	ThruPLEX DNA-Seq Kit	96.7	9.7
Myrmecocichla aethiops	MVZ, 129113	Toepad	ACCEL-NGS 1S DNA Library Prep Kit	93.3	6.8
Myrmecocichla arnotti	FMNH, 468111	Toepad	Illumina DNA Prep Kit	99.3	12.8
Myrmecocichla formicivora	MVZ, RSA205	Muscle	Illumina DNA Prep Kit	98.6	8.3
Myrmecocichla melaena	A1153	Blood	ThruPLEX DNA-Seq Kit	98.8	13.3
Myrmecocichla monticola	NMBE, 1043860	Toepad	ACCEL-NGS 1S DNA Library Prep Kit	94.3	7.6
Myrmecocichla nigra	NRM, 570041	Toepad	ThruPLEX DNA-Seq Kit	94.5	7.0
Myrmecocichla tholloni	YPM, ORN95640	Toepad	ThruPLEX DNA-Seq Kit	92.1	7.3
Oenanthe (C.) dubia	FMNH, 83201	Toepad	ACCEL-NGS 1S DNA Library Prep Kit	93.0	6.8
Oenanthe (C.) familiaris	MVZ, GO866	Blood	Illumina DNA Prep Kit	99.4	13.3
Oenanthe (C.) fusca	YPM, ORN011707	Toepad	ThruPLEX DNA-Seq Kit	86.4	4.7
Oenanthe (C.) melanura	A1203	Blood	ThruPLEX DNA-Seq Kit	98.8	15.4
Oenanthe (C.) scotocerca	LACM, 61131	Toepad	ACCEL-NGS 1S DNA Library Prep Kit	96.6	8.3
Oenanthe (M.) albifrons clericalis	NRM, 558941	Toepad	ThruPLEX DNA-Seq Kit	95.4	6.3
Oenanthe (M.) albifrons frontalis	KU, 115365	Muscle	ThruPLEX DNA-Seq Kit	98.5	12.7
Oenanthe albonigra	IR-KIL-010	Blood	ThruPLEX DNA-Seq Kit	99.2	12.9
Oenanthe bottae frenata	NRM, 558917	Toepad	ThruPLEX DNA-Seq Kit	97.0	6.0
Oenanthe chrysopygia	IR-FIR-002	Blood	ThruPLEX DNA-Seq Kit	98.9	11.5
Oenanthe cypriaca	19e	Blood	Chromium Genome Library kit	99.8	40.6
Oenanthe deserti	MO-BOULMANE-2013	Blood	ThruPLEX DNA-Seq Kit	99.3	12.6
Oenanthe finschii	IR-ESF-004	Blood	ThruPLEX DNA-Seq Kit	98.9	8.7
Oenanthe halophila	3Y42902	Blood	Illumina DNA PCR-free	99.6	17.4
Oenanthe heuglinii	ZFMK, H.II.16p2.α	Dry skin	ACCEL-NGS 1S DNA Library Prep Kit	93.6	5.7

Oenanthe hispanica	E-GUI-013	Blood	Chromium Genome Library kit	99.8	15.5
Oenanthe isabellina	GR-LES-001	Blood	ThruPLEX DNA-Seq Kit	99.2	9.9
Oenanthe leucopyga leucopyga	A1137	Blood	ThruPLEX DNA-Seq Kit	98.8	10.7
Oenanthe leucura leucura	E-MAT-2012	Blood	ThruPLEX DNA-Seq Kit	99.0	9.5
Oenanthe lugens lugens	9b	Blood	ThruPLEX DNA-Seq Kit	98.7	22.0
Oenanthe lugens persica	ZMUC, 137759	Muscle	ThruPLEX DNA-Seq Kit	98.6	10.4
Oenanthe lugentoides lugentoides	NHMUK, 1965.M.12140	Toepad	ThruPLEX DNA-Seq Kit	96.9	4.6
Oenanthe lugentoides boscaweni	NHMUK, 1977.M.21.36	Toepad	ThruPLEX DNA-Seq Kit	97.2	6.8
Oenanthe lugubris lugubris	A1129	Blood	ThruPLEX DNA-Seq Kit	99.0	12.5
Oenanthe lugubris vauriei	AMNH, 461151	Toepad	ThruPLEX DNA-Seq Kit	95.9	5.3
Oenanthe melanoleuca	IT-GRA-006	Blood	Chromium Genome Library kit	99.7	12.6
Oenanthe moesta	A1109	Blood	ThruPLEX DNA-Seq Kit	98.8	12.0
Oenanthe monacha	A1174	Blood	ThruPLEX DNA-Seq Kit	99.3	17.2
Oenanthe oenanthe	GEO-VAR-002	Blood	ThruPLEX DNA-Seq Kit	99.1	12.2
Oenanthe phillipsi	YPM, ORN035210	Toepad	ThruPLEX DNA-Seq Kit	95.6	7.9
Oenanthe picata capistrata	ZMUC, 29495	Toepad	ThruPLEX DNA-Seq Kit	96.7	5.3
Oenanthe picata opistholeuca	ZMUC, 29578	Toepad	ThruPLEX DNA-Seq Kit	97.1	5.2
Oenanthe picata picata	IR-TAN-005	Blood	ThruPLEX DNA-Seq Kit	98.8	14.2
Oenanthe pileata	TCWC, 15606	Muscle	Illumina DNA Prep Kit	98.9	13.4
Oenanthe pleschanka	CN-XS-006	Blood	Chromium Genome Library kit	99.8	15.1
Oenanthe seebohmi	KA69373	Blood	ThruPLEX DNA-Seq Kit	99.2	11.2
Oenanthe warriae	12c	Blood	ThruPLEX DNA-Seq Kit	98.7	13.4
Oenanthe xanthoprymna	NHMO, 15188	Blood	ThruPLEX DNA-Seq Kit	99.0	12.9
Pinarochroa sordida	YPM, ORN80066	Toepad	ThruPLEX DNA-Seq Kit	95.4	6.5
Thamnolaea cinnamomeiventris	NRM, 20086147	Muscle	ThruPLEX DNA-Seq Kit	98.6	15.9

[a] AMNH; American Museum of Natural History; NHMUK: Natural History Museum, Tring; FMNH: Field Museum of Natural History; LACM: Natural History Museum of Los Angeles County; MVZ: Museum of Vertebrate Zoology, UC Berkeley; NHMO: Natural History Museum, University of Oslo; NRM: Naturhistoriska riksmuseet, Stockholm; TCWC: Texas A&M University Biodiversity Research and Teaching Collections; UWBM: University of Washington Burke Museum; YPM: Yale Peabody Museum; ZMUC: Zoological Museum, Natural History Museum of Denmark; ZFMK: Zoologisches Forschungsmuseum König. Samples for which no institution is indicated are part of the research group's collection.

Figure captions

Figure 1 | Time-calibrated phylogenetic tree of open-habitat chats and levels of ILS. All nodes are supported by bootstrap values of 100. Pie charts depict the gene tree heterogeneity for each internal branch, with the brown proportion indicating the proportion of concordant gene trees (gCF). Coloured branches indicate internal branches for which ILS alone is statistically sufficient to explain the observed gene tree heterogeneity. Stars indicate branches that are in the phylogenetic anomaly zone. The character states of three selected characters: Sexual dimorphism (SD), monomorphic female-type (white), monomorphic male-type (pale green), dimorphic (dark green); Migratory behaviour (Mig), sedentary (white), short-distance migrant (pale green), long-distance migrant (dark green); and throat coloration (throat), white (white), black (pale green), and polymorphic (white and pale green). Drawing courtesy of Chris Rose (www.chrisrose-artist.co.uk) with permission from Bloomsbury Publishing Plc.

Figure 2 | Mito-nuclear discordances. Shown are the time-calibrated phylogenetic trees based on nuclear data (left) and full mitogenomes (right).

Figure 3 | Footprints of introgression as estimated by the f-branch statistic. The heat map summarizes the f-branch statistics estimated in Dsuite. Darker colors depict increasing evidence for gene flow between lineages. Dotted lines in the phylogeny represent ancestral lineage.

Figure 4 | Phylogenomic networks and distribution ranges for the *picata* (left), *lugens* (middle) and *hispanica* (right) complexes. Phylogenomic networks were estimated under the maximum pseudolikelihood approach implemented in phyloNet. Numbers on the edges indicate the inheritance probabilities, which correspond to the proportion of gene trees supporting the reticulate relationship. Drawings courtesy of Chris Rose (www.chrisrose-artist.co.uk) with permission from Bloomsbury Publishing Plc. Distribution ranges modified from BirdLife International and the Handbook of the Birds of the World (2016).

1131

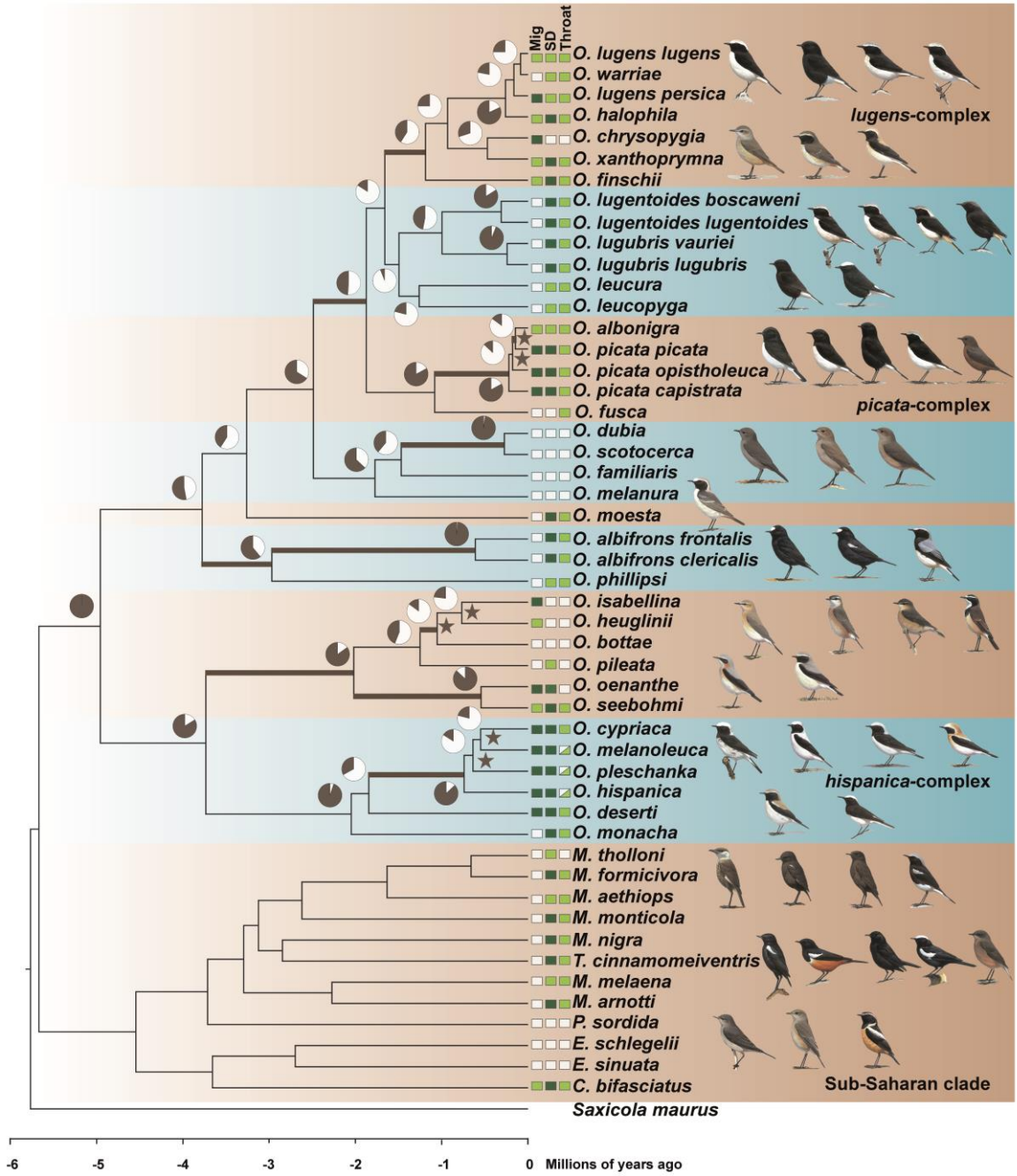

Figure 1 | Time-calibrated phylogenetic tree of open-habitat chats and levels of ILS. All nodes are supported by bootstrap values of 100. Pie charts depict the gene tree heterogeneity for each internal branch, with the brown proportion indicating the proportion of concordant gene trees (gCF). Coloured branches indicate internal branches for which ILS alone is statistically sufficient to explain the observed gene tree heterogeneity. Stars indicate branches that are in the phylogenetic anomaly zone. The character states of three selected characters: Sexual dimorphism (SD), monomorphic female-type (white), monomorphic male-type (pale green), dimorphic (dark green); Migratory behaviour (Mig), sedentary (white), short-distance migrant (pale green), long-distance migrant (dark green); and throat coloration (throat), white (white), black (pale green), and polymorphic (white and pale green). Drawing courtesy of Chris Rose (www.chrisrose-artist.co.uk) with permission from Bloomsbury Publishing Plc.

1132

1133

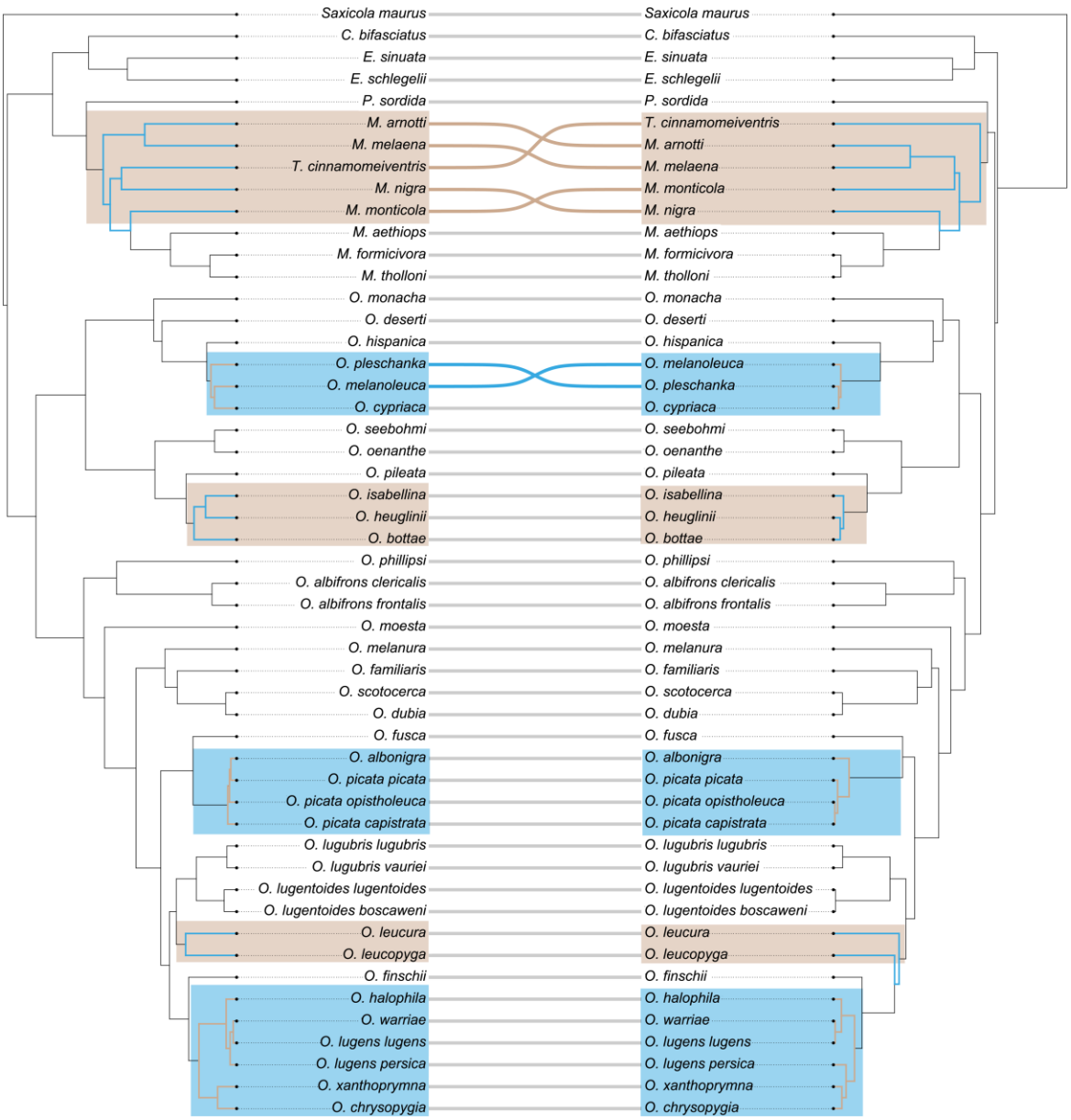

Figure 2 | Mito-nuclear discordances. Shown are the time-calibrated phylogenetic trees based on nuclear data (left) and full mitogenomes (right).

1134

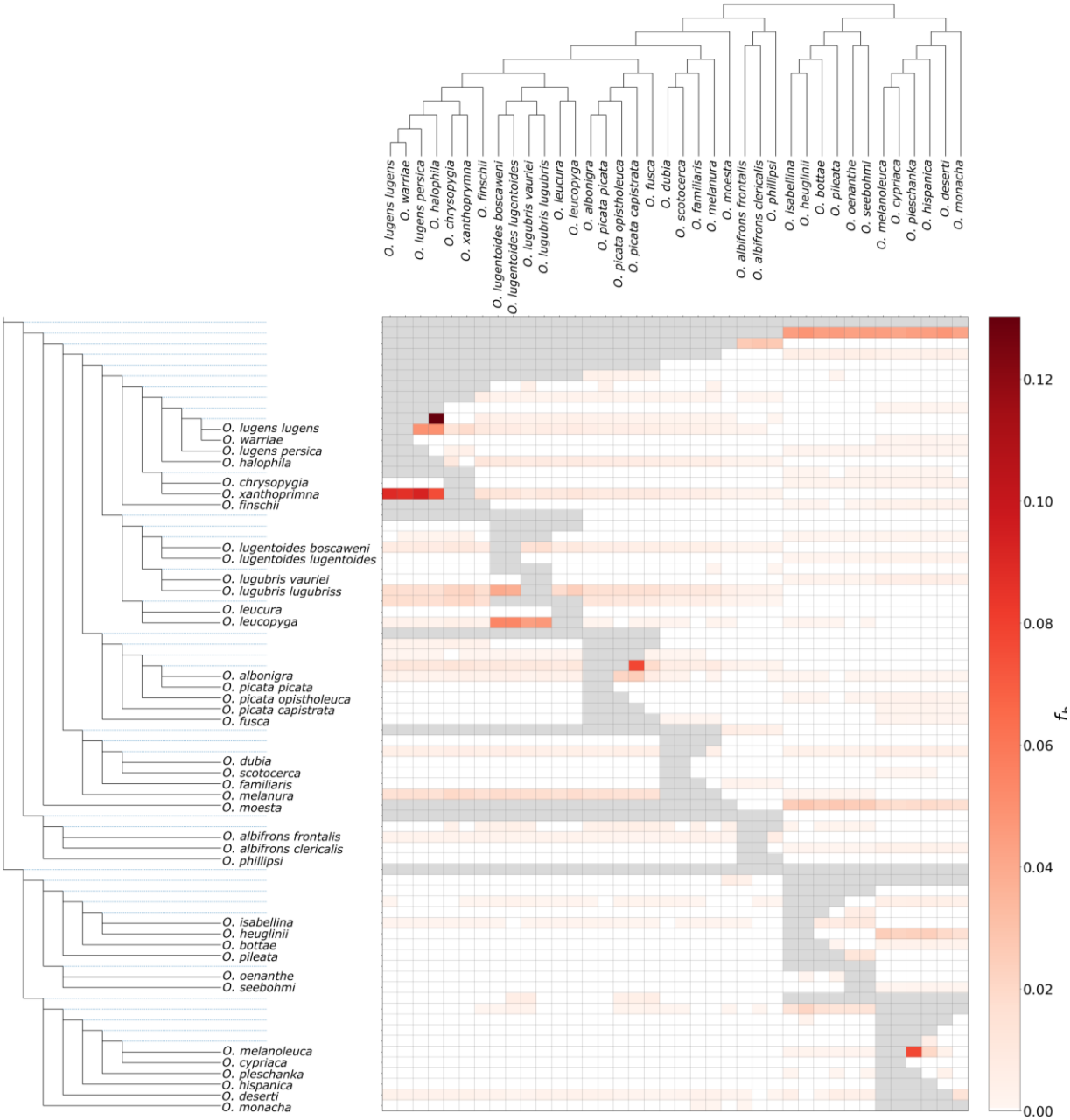

Figure 3 | Footprints of introgression as estimated by the f-branch statistic. The heat map summarizes the f-branch statistics estimated in Dsuite. Darker colors depict increasing evidence for gene flow between lineages. Dotted lines in the phylogeny represent ancestral lineage.

1135

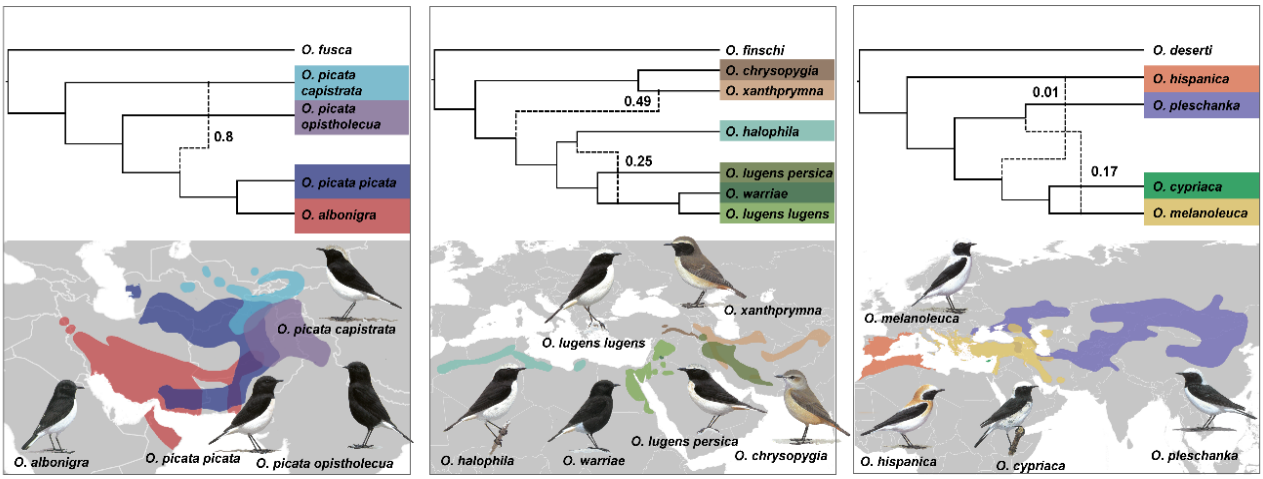

Figure 4 | Phylogenomic networks and distribution ranges for the *picata* (left), *lugens* (middle) and *hispanica* (right) complexes. Phylogenomic networks were estimated under the maximum pseudolikelihood approach implemented in phyloNet. Numbers on the edges indicate the inheritance probabilities, which correspond to the proportion of gene trees supporting the reticulate relationship. Drawings courtesy of Chris Rose (www.chrisrose-artist.co.uk) with permission from Bloomsbury Publishing Plc. Distribution ranges modified from BirdLife International and the Handbook of the Birds of the World (2016).

Supplementary tables

Table S1 | Number of loci across the genome using different filtering settings for 10 kb non-overlapping windows: minimum read depth (DP), minimum percentage of the window covered by data (PW), and missing data per site (MD).

Filtering setting	Number of total windows	Number of no intra-locus recombination windows	Number of no intra-locus and free inter-locus recombination windows
DP=1, PW=50%, MD=15%	29,730	10,051	6,791
DP=5, PW=50%, MD=15%	19,062	6,701	5,788
DP=1, PW=50%, MD=5%	26,030	9,600	6,476
DP=1, PW=80%, MD=10%	22,652	6,970	5,267

Table S2 | Selection of the best models among the maximum pseudo-likelihood networks in phyloNet 3.6.9.

Complex	**Gene trees**	**Inferred admixtures**	**Likelihood**	**BIC**
O. picata	7,310	0	-33,633.58	67,278.88
		1	**-33,559.56**	**67,131.21**
		2	-33,569.10	67,150.56
		3	-33,617.49	67,247.56
		4	-33,979.37	67,971.48
		5	-33,982.37	67,977.62
O. hispanica	7,335	0	-33,326.92	66,665.57
		1	-33,180.89	66,373.86
		2	**-33,153.96**	**66,320.28**
		3	-33,265.29	66,543.14
		4	-33,276.89	66,566.51
		5	-33,637.19	67,287.26
O. lugens	,7323	0	-86,457.1	17,2926.3
		1	-85,643.3	17,1299.0
		2	**-85,014.9**	**17,0042.3**
		3	-86,498.8	17,3010.4
		4	-86,574.7	17,3162.3
		5	-86,095.2	17,2203.3

Supplementary Figures

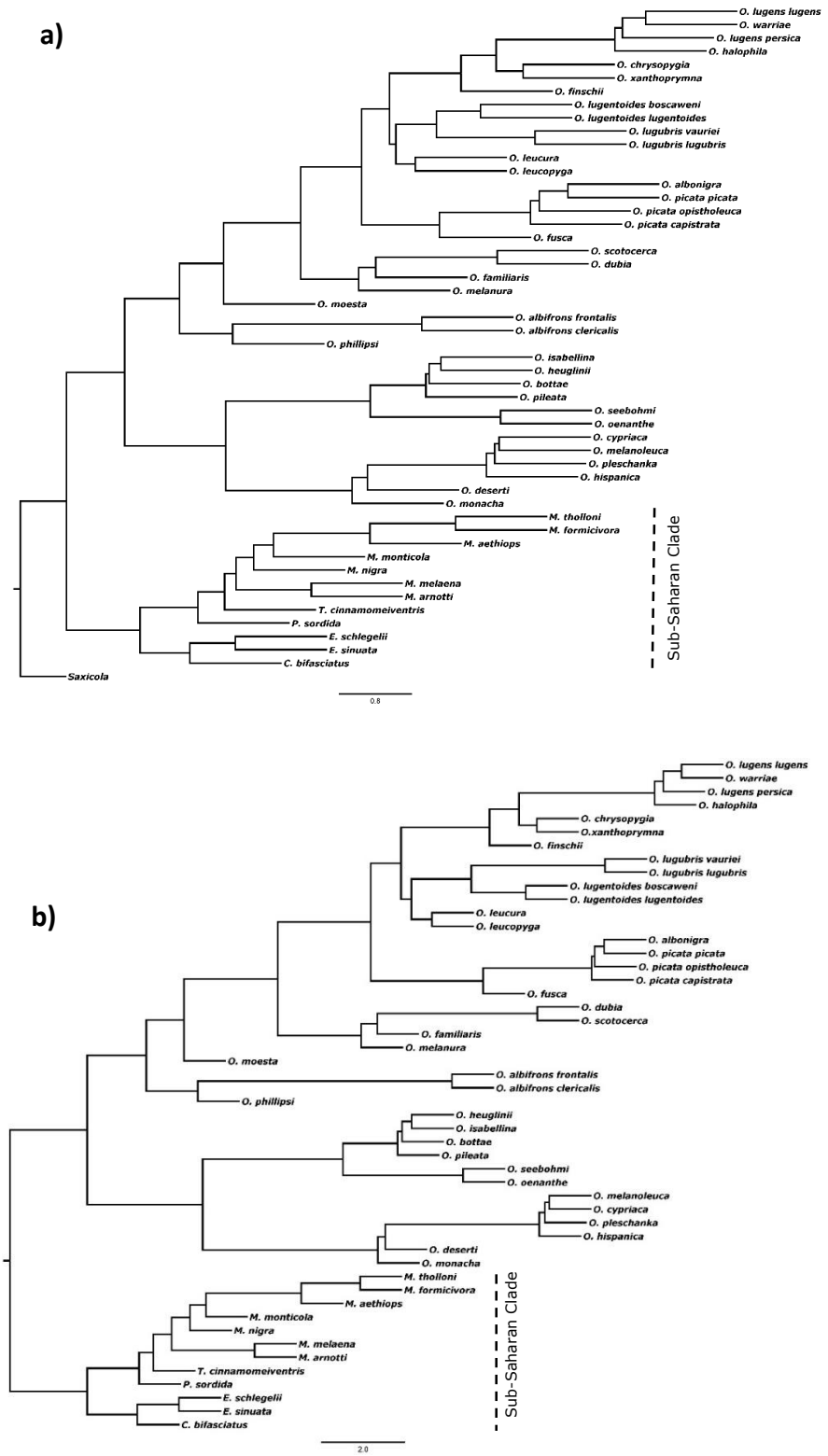

Figure S1 | Genome-wide multispecies coalescent species tree of open-habitat chats estimated in ASTRAL-III. All nodes have 1.0 local posterior probabilities. a) Species tree based on 2,091 BUSCOs, using *Saxicola* as an outgroup. b) Species tree based on 5,788 loci (non-overlapping 10 kb windows across the genome) using the sub-Saharan clade as an outgroup.

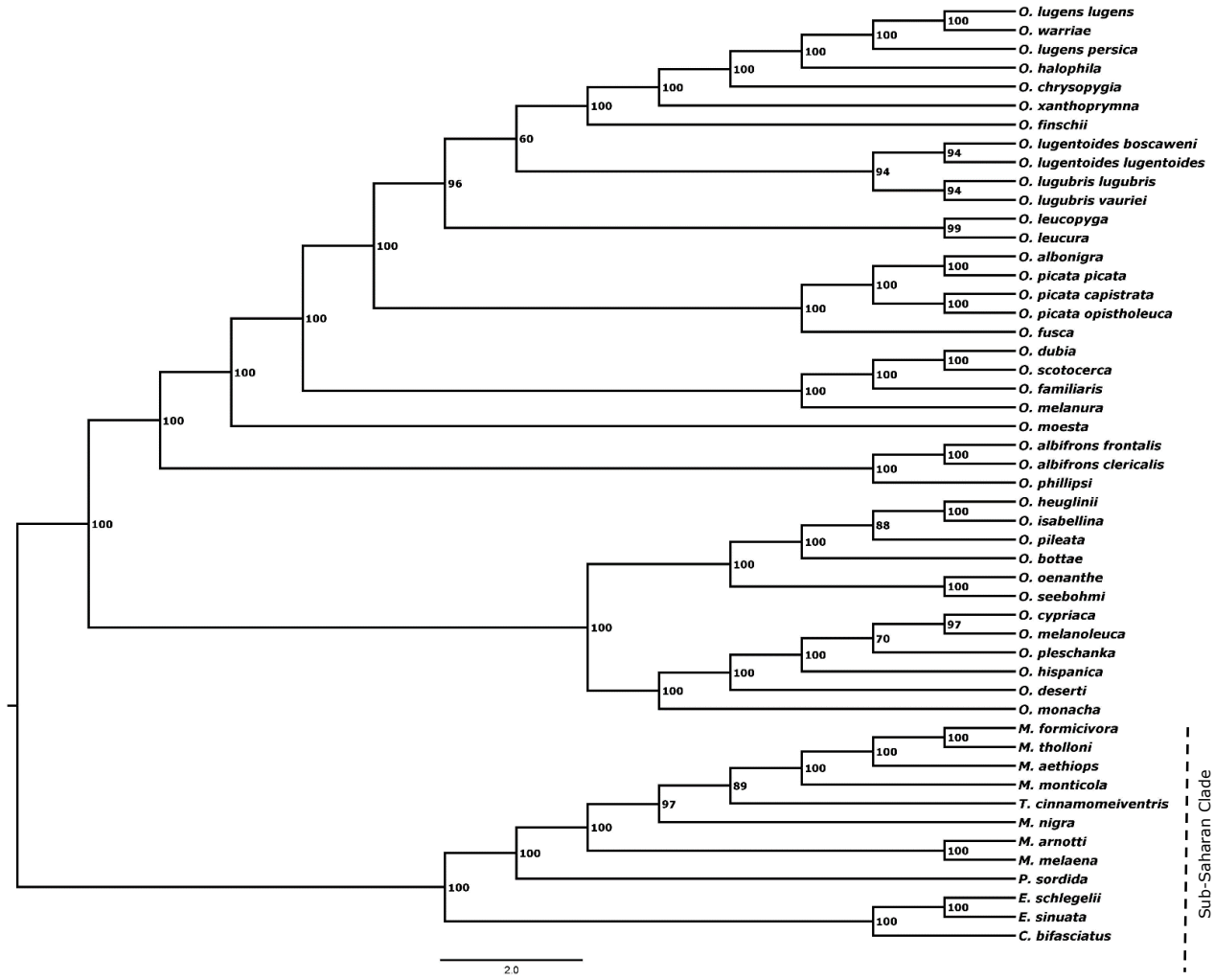

Figure S2 | SNP-based multispecies coalescent species tree of open-habitat chats inferred with SVDquartets in PAUP* 4. Maximum likelihood bootstrap support values are shown above branches.

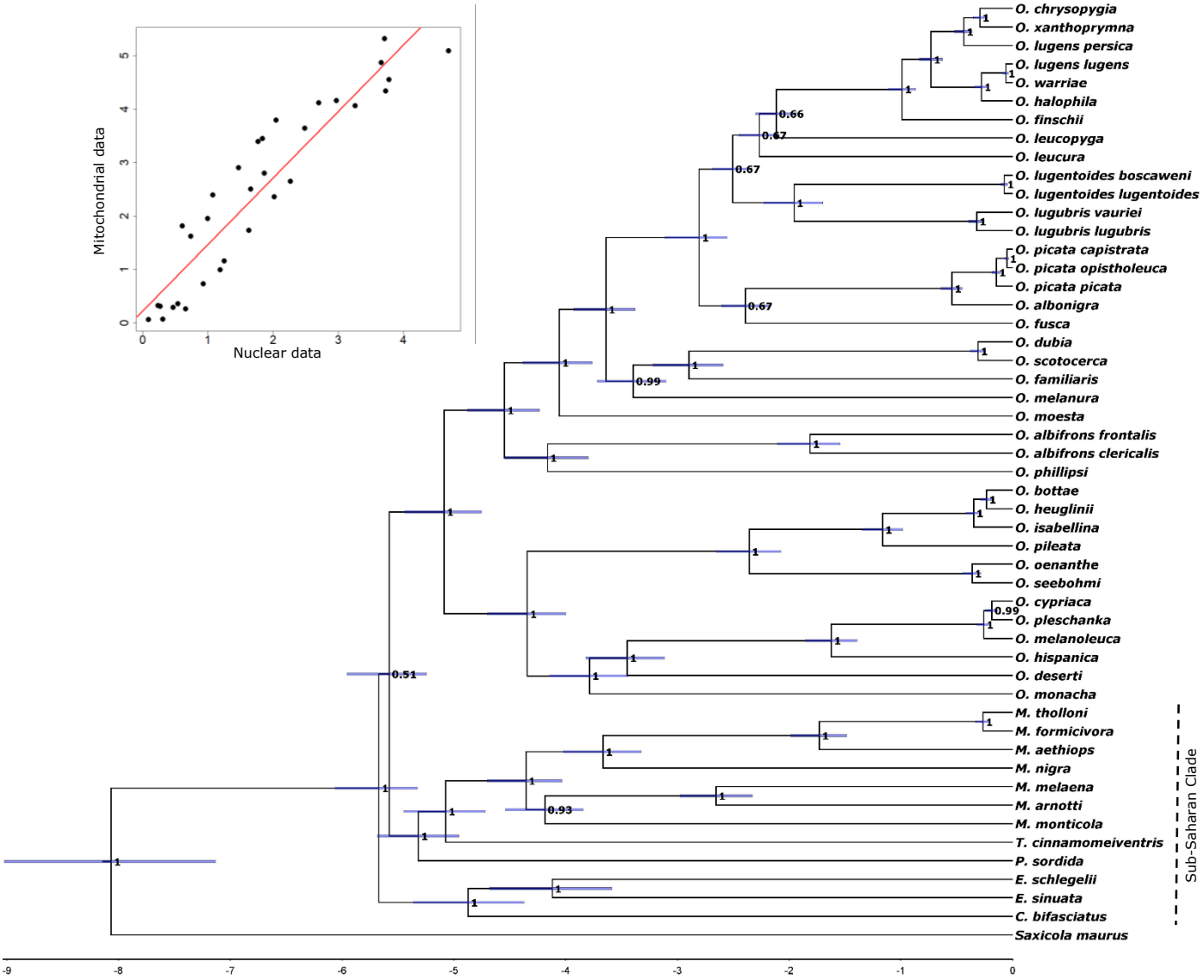

Figure S3 | Time-calibrated maximum clade credibility tree of the BEAST 2.6.6 analyses based on 13 protein-coding mitochondrial genes of open-habitat chats. Blue bars represent the 95% highest posterior density (HPD) distributions for the estimated divergence times. Posterior probabilities are indicated at nodes. The correlation between the dating based on the nuclear (BUSCOs) and mitochondrial data is shown at the top left (Pearson's r=0.93, p<0.001).

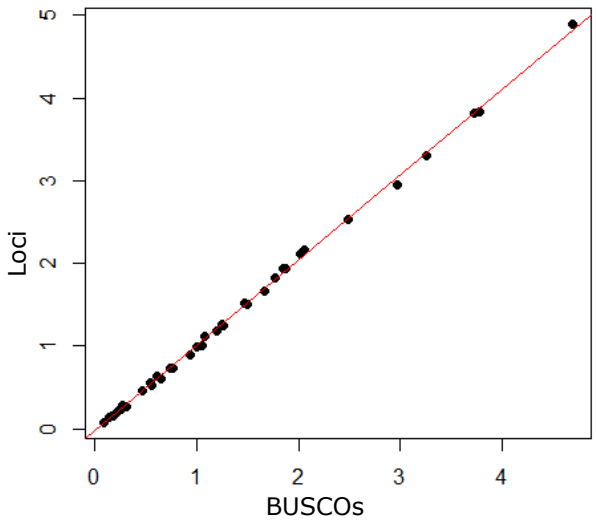

Figure S4 | Correlation between the time calibration based on 1.8 Mb high confidence BUSCOs and 3.8 Mb high confidence loci (10 kb non-overlapping windows across the genome) using RelTime-ML implemented in MEGA 11 (Pearson's r=0.99, p<2.2e-16).

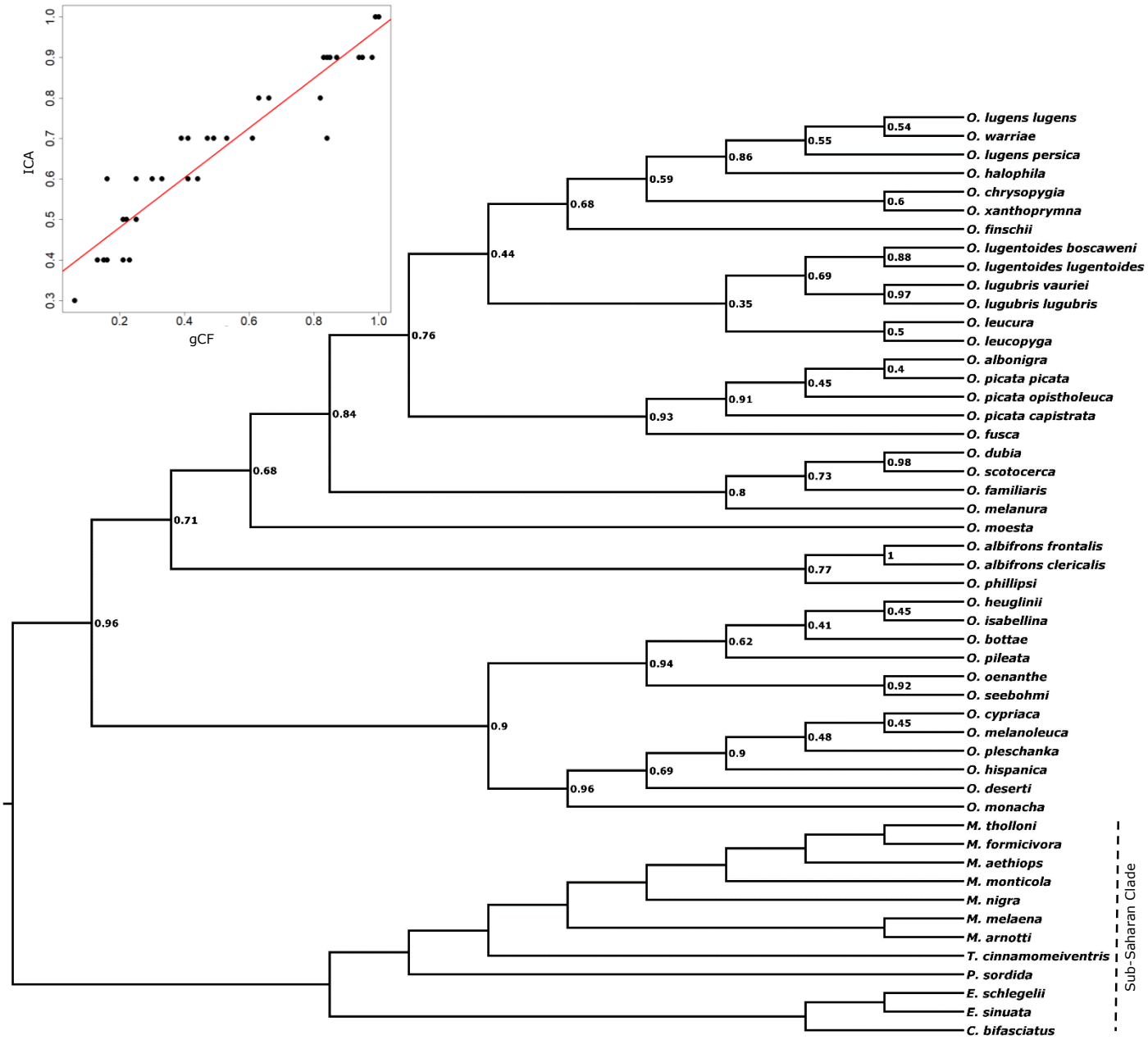

Figure S5 | Genome-wide multispecies coalescent species tree of open-habitat chats estimated in ASTRAL-III. ICA values for 29,730 maximum-likelihood gene trees are shown for each node. The high correlation between the gCF values calculated in IQ-TREE 2.1.2 and ICA values calculated in PhyParts 0.0.1 is shown at the top left (Pearson's r=0.94, p<0.001).